PHY 453

CHARACTERISATION OF DEFECTS IN SILICON USING FTIR ABSORPTION SPECTROSCOPY

By

Muhammad Abdul Rauf Khan

A thesis submitted in partial fulfilment of the requirement for the degree of

Master of Philosophy

in

Physics

Semiconductor Physics Laboratory

Department of Physics

Quaid-i-Azam University

Islamabad, Pakistan

June 2000

Dedicated to My Parents

CERTIFICATE

Certified that the work reported in this thesis has been carried out in Semiconductor Physics Laboratory by **Mr. Muhammad Abdul Rauf Khan** under my supervision.

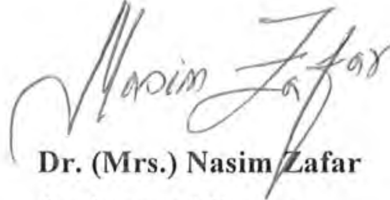

Dr. (Mrs.) Nasim Zafar

Professor of Physics
Semiconductor Physics Laboratory
Department of Physics
Quaid-i-Azam University
Islamabad, Pakistan

Submitted through

Prof. Dr. M. Zafar Iqbal

Chairman
Department of Physics
Quaid-i-Azam University
Islamabad, Pakistan

ACKNOWLEDGEMENTS

All praises and thanks are for Almighty Allah who is the source of all knowledge and wisdom endowed to mankind, and to the Holly Prophet Muhammad (peace be upon him) who is forever a torch of guidance for humanity as a whole.

I am much indebted to my supervisor Prof. Dr. (Mrs.) Nasim Zafar for her guidance and valuable suggestions during this work. I wish to thank her for all that she has done for me.

I offer my extreme gratitude to Prof. Dr. M. Zafar Iqbal who has always been a source of knowledge and guidance for me. His guidance has made it possible for me to complete this work. I would like to thank Dr. Umar Saeed Qurashi for giving me help during my experimental work. I would like to offer my cordial thanks to all my research fellows in Semiconductor Physics Laboratory especially Mr. Abdul Majid and Mr. Shah Haidar Khan for their help and enjoyable company during my research work. I am thankful to all my other friends who have given me company during my stay at Quaid-i-Azam University.

I am extremely thankful to my father for providing me financial and moral support during my M. Phil course. At last and not the least I am indebted to my mother and sisters for their prayers and best wishes for my success.

Muhammad Abdul Rauf Khan

ABSTRACT

The work presented in this dissertation comprises a study of the infrared absorption characteristics of the vibrational modes in silicon using FTIR spectroscopy in the wavenumber range 4600-400 cm^{-1}. All the measurements were performed at room temperature with the spectral resolution of 1 cm^{-1}. Silicon samples used in this investigation were grown by two different growth techniques, Czochralski (CZ) and Float-zone (FZ) techniques.

The FTIR absorption spectra are divided into two categories. The category A consists of the spectra obtained on the float-zone samples and category B is the spectra obtained on the sample grown by Czochralski technique. The FTIR spectra of our silicon samples show some important features in the spectral range from 1400-400 cm^{-1}. On the basis of the comparison with the available literature, we conclude that our samples show the well known absorption peaks due to the substitutional carbon (Cs), interstitial oxygen (Oi), B^{11} and (B^{11}-Sb). Some other, smaller peaks have also been observed by us.

LIST OF CONTENTS

Chapter 1	**Introduction**			
1.1	Spectroscopy and Electromagnetic Radiation			2
1.2	Infrared Spectroscopy			3
1.3	Infrared Spectroscopy of Crystals			5
1.4	Infrared Spectroscopy of Semiconductors			7
1.5	Motivation of This Project			8
Chapter 2	**Theory of Fourier Transform Infrared Spectroscopy**			
2.1	Optics of Fourier Transform Infrared Spectrometer			11
2.2	Apodization			14
2.3	Resolution			17
2.4	Beam Splitter			18
2.5	Advantages of FTIR Spectroscopy			19
	1	Throughput Advantage		20
	2	Multiplex Advantage		21
	3	Laser Reference Advantage		21
2.6	Applications of FTIR Spectroscopy			22
Chapter 3	**Experimental Details**			
3.1	Samples			24
	3.1.1	Czochralski Crystal Growth Technique		24
	3.1.2	Float-Zone Technique		26
3.2	Experimental Set-Up			28
	1	Compressor-Dryer System		28
	2	Fourier Transform Infrared (FTIR) Spectrometer System		29
		1	The Optical System	29
		2	The Data System	31
3.3	The Data Collection			31
	3.3.1	Background Measurements		31
	3.3.2	Sample Measurements		43
		(i)	Resolution	43
		(ii)	Detector Gain	43

(iii) Mirror Velocity 44
(iv) Number of Scans 44
(v) Apodization Function 44
3.4 Baseline Correction of Spectra 46
(i) Curve Correction 46
(ii) Ramp Correction 47
(iii) Level Correction 47
3.5 Storage/Retrieval of Data 47
3.6 Plotting the Data 48
Chapter 4 Results & Discussion
4.1 Introduction 49
4.2 Results and Analysis 50
4.2.1 A: Float-Zone Silicon 50
1 p-type Silicon (p Si 106 FZ sample) 50
2 n-type Silicon 54
3 Si High Carbon Low Oxygen (Si HCLO sample) 62
4 (i) Si-Reference Ultra High Purity Oil Quenched Sample 62
(ii) Si-Ag UHP Oil Quenched Sample 62
5 Si 30994/64 FZ Sampe 70
4.2.2 B: Czochralski (CZ) Silicon Sample (Silicon 522 Big) 70
4.3 Discussion 76
4.3.1 Effects of Oxygen Concentration on Vibrational Modes 76
4.3.2 Effects of Carbon Concentration on Vibrational Modes 77
4.3.3 Five Smaller Peaks 78
4.3.4 The 610 cm^{-1} Peak 78
4.4 Conclusions 79
References 81

CHAPTER 1

INTRODUCTION

A very interesting area of research in of semiconductors is the study of defects in semiconductor materials. Since defects play a very important role in the characteristics of a semiconductor. Over the years, many physicists have devoted a major portion of their professional career using classical methods involving qualitative and quantitative analysis. Classical methods are not only time consuming but sometimes also ambiguous. Chemists also encounter with such problems. Their problems include isolation and purification of components of a mixture and structural determination of individual unknown components.

With the advancement of instrumental techniques, e.g., ultraviolet, infrared, NMR and mass spectroscopy, the organic chemical practice has been revolutionized. Such techniques not only help in achieving the results, which were difficult otherwise but also achieve them faster. Each instrumental technique provides a specific information about the structure of a molecule, for example ultraviolet spectrophotometry has special use in the structural determination of compounds containing unsaturation or conjugation. Ultraviolet or visible spectrum is useful because the promotion of electrons from ground state to the excited state of a material gives rise to absorption in this region. Infrared spectroscopy is used to detect and identify the molecular vibrations, specially the characteristic vibrations of double and triple bonds such as C-H, N-H, O-H, C≡N, C≡C, C=O and C-O are present in a molecule or not. Nuclear magnetic resonance (NMR) technique detects changes in the alignment of a nuclear magnet in a strong magnetic field. Absorption is observed from, with either odd atomic number or odd mass number. The precise frequency of

absorption is a very sensitive measure of the magnetic and hence the chemical environment of such nuclei. Mass spectroscopy measures the mass- to-charge ratio of organic ions created by electron bombardment. All these instrumental techniques fall under the domain of spectroscopy.

1.1 Spectroscopy and Electromagnetic Radiation

Spectroscopy can be defined as, the interaction of radiation with matter. Thus, the knowledge of electromagnetic radiation, their classification on the basis of energy and the energy levels of the molecules, is essential to understand spectroscopy.

There are different types of electromagnetic radiation such as cosmic rays, gamma rays, x-rays, ultraviolet rays, visible and infrared rays, microwaves and radio waves. These electromagnetic radiation move with the velocity of light. It is possible to differentiate between these electromagnetic radiation on the basis of either frequency (ν) or wavelength (λ) using the equation $c = \nu\lambda$. Thus x-rays have the highest frequency and the shortest wavelength, where as radio waves have maximum wavelength and the lowest frequency. Higher frequency radiation have high energy and vice versa. Wavelength of radio waves is measured in meters, microwaves in centimeters (cm), infrared in micrometers (μm), visible and ultraviolet in nanometers (nm) and that of x-rays in angstrom (A^o). The energy associated with each radiation is computed from the relation,

$$\mathbf{E = h\nu = hc/\lambda}$$

It is customary to express radio waves in frequency unit i.e. KHz and MHz, infrared in wavenumber (v) and ultraviolet in wavelength units (nm) and x-rays in angstrom (A^o).

Thus different regions of electromagnetic radiation provide sufficient energy to study specific changes in molecules. Each spectroscopic technique i.e. UV, IR, NMR and mass spectroscopy, gives specific information about the structure of a compound [1].

1.2 Infrared Spectroscopy

We need three independent coordinates to describe the position of the free atom, and such an atom is accordingly said to have three degrees of freedom. An assembly of N atoms has 3N degree of freedom, three for each atom. When the N atoms are linked together in a molecule , there are still 3N degrees of freedom for the system, but it is more appropriate in this situation to consider them in terms of the molecule as a whole instead of in terms of the individual atoms. Thus we can regard the molecule itself as having three degrees of translational freedom, corresponding to the three coordinates needed to describe the position of its center of mass, and if it is a nonlinear molecule, it also has three degrees of rotational freedom, corresponding to three angular coordinates needed to describes orientation in space. The remaining 3N-6 degrees of freedom refer to changes to relative positions of the atoms within the molecule; they are the internal degrees of freedom. Because the rotation about the symmetry axis of a linear molecule can be ignored, there are only two degrees of rotational freedom for such a molecule and 3N-5 internal degrees of freedom.

Each internal degree of freedom in a molecule corresponds to a particular mode of vibration. Some of these modes involve the stretching and compressing of bonds and the rest involve bending or distorting the molecule. A diatomic molecule is linear and has N=2, and since 3N-5 = 1 , there is only a single internal degree of

freedom and only one mode of vibration. The H_2O molecule is nonlinear and therefore has 3N-6 = 3 modes of vibration [2].

A bond in an organic molecule may stretch or it may bend relative to other bonds. The stretching vibration is one in which the inter-nuclear distance of two atoms increases or decreases, but the atoms remain in the same bond axis, where as in a bending vibration the position of the atoms changes relative to the original bond axis. Different modes of vibrations of a bond in a molecule are shown below.

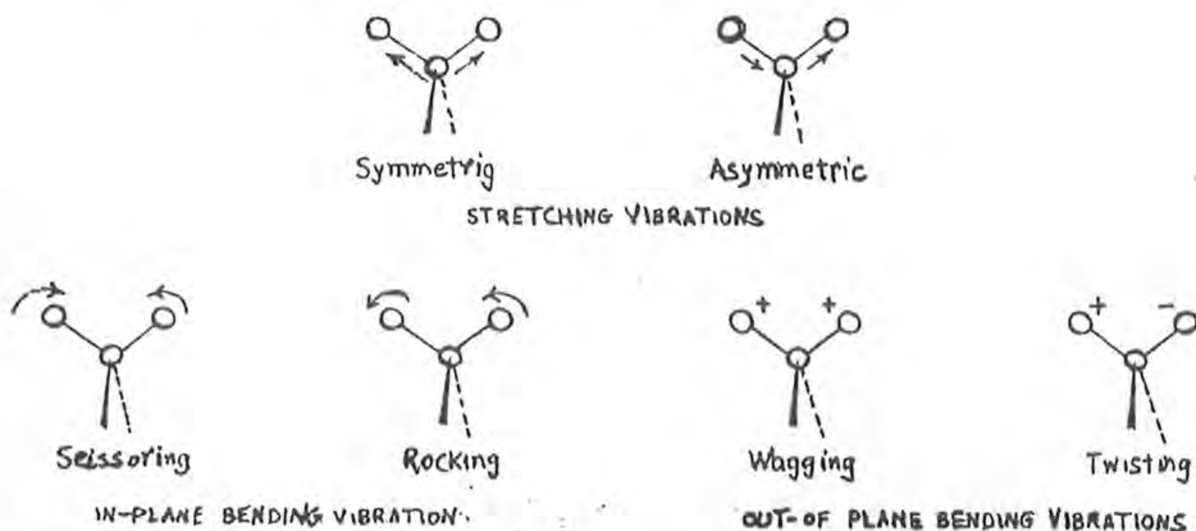

Fig. 1.1 Modes of vibrations of a bond in a molecule

For the occurrence of each stretching or bending vibration in a molecule a definite quantum of energy is required. This quantum of energy is provided by infrared part of electromagnetic radiation. Out of many possible stretching or bending vibrations, only those vibrations are capable of absorbing infrared radiation which cause a change in the dipole moment. Bending vibrations occur at longer wavelength than stretching vibrations [1].

Infrared spectroscopy has been a useful technique for materials analysis in the laboratory for over seventy years. An infrared spectrum represents a fingerprint of a sample with absorption peaks which correspond to the frequency of vibrations of the bonds of the atoms making up the material. Because each different material is a unique combination of atoms, no two compounds produce the exact same infrared spectrum. Therefore, infrared spectroscopy can result in a positive identification of every different kind of materials. In addition, the size of the peaks in the spectrum is a direct indication of the amount of material present in a sample [3].

1.3 Infrared Spectroscopy of Crystals

The presence of a point defect in an otherwise perfect crystal destroys the translational symmetry of the lattice and at the same time modifies its normal modes of vibrations. There are two possibilities, (1) all the modified modes lie within the bands of perfect lattice frequencies (band modes) and any disturbance of the system involving the defect can be transmitted through out the crystal, or (2) certain new modes occur at frequencies greater than the maximum perfect lattice frequency (localized modes) or between bands of allowed frequencies (gap modes), disturbances at either of these two latter frequencies can not be propagated and are highly localized spatially around the defect. The calculation of these effects is a problem in a lattice dynamics and requires a knowledge of normal modes of vibration of the perfect crystal and the precise nature of the point defect. The simplest defect consists of an isolated substitutional impurity atom of known mass.

The localized modes of vibration occur when the defect consists of an impurity atom which is somewhat lighter than the atom of the host crystal, provided the force constants between this atom and its neighbours have a similar strength to those between pairs of host crystal atoms. The introduction of a heavier atom, or a light atom with weak force constants usually leads to modified band modes only. Different methods have been used for the experimental observation of these effects. The most direct method is to measure the infrared absorption induced by the presence of the defects. Not only are the localized modes infrared active but also the spectrum of perturbed band modes, because of the removal of the translational symmetry of the lattice. The coupling of the incident radiation to various modes depend upon a dipole moment which is itself frequency dependent. So the observed band mode absorption does not in general show the density of lattice modes but depends on the particular defect which is present.

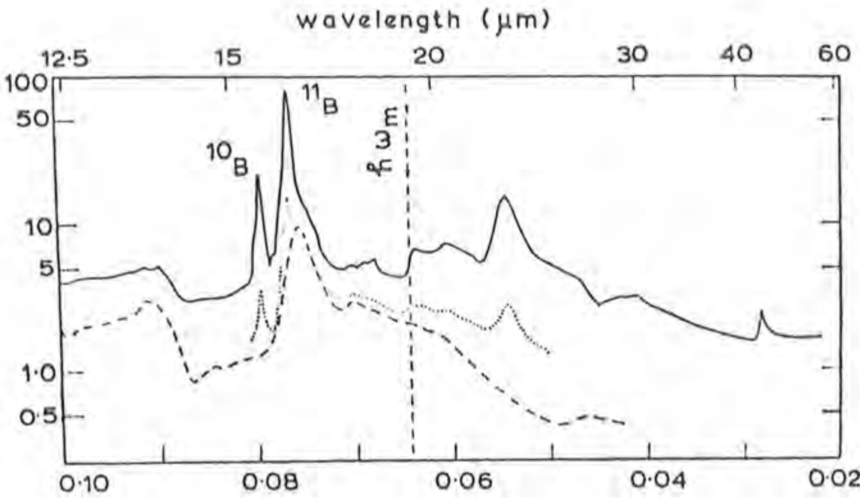

Fig. 1.2 The infrared absorption spectrum (290 K) of silicon doped with both boron (B^{10}+B^{11}) and phosphorus in concentration of 5×10^{19} cm^{-3} (full curve) and 5×10^{18} cm^{-3} (dotted curve); the spectrum of pure silicon (dashed curve) is shown for comparison [4].

These effects are well illustrated by the observation on compensated silicon containing boron (B^-) and phosphorus(P^+) ions. The presence of light boron ions consisting of a mixture of isotopes with masses ten and eleven, gives rise to two distinct localized modes of vibrations, one for each isotope. These are shown in Fig. 1.2.

1.4 Infrared Spectroscopy Of Semiconductors

In infrared spectroscopy , IR radiation is passed through a sample. Some of the infrared radiation is absorbed by the sample and some of it is passed through (transmitted). The resulting spectrum represents the molecular absorption and transmission, creating a molecular fingerprint of the sample. Like a fingerprint no two unique molecular structures produce the same infrared spectrum.

In a semiconductor, atoms are bonded together via covalent bonds. In elemental semiconductors such as Si, Ge, C and α–Sn, there is a tetrahedral bonding between the atoms, i.e. each atom has four nearest neighbors. Since no element can be totally purified, impurities are always present. For example , in silicon, which is probably one of the most pure materials available, it is common for there to be a measurable amount of carbon and oxygen present. Carbon normally occupies substitutional sites(Cs), it is electrically inactive and has a local phonon frequency, as detected by infrared absorption measurements. Oxygen, on the other hand, is interstitially (O_i) incorporated in the silicon lattice occupying positions between two nearest neighbour Si atoms. However, it has also been suggested [5] that O could also occupy substitutional sites in the silicon Lattice. The presence of Oi is manifested by the absorption band at 1205,1106, 515 cm^{-1}. It is suggested that Oi may be forming chain-like structures in the Si lattice [6].

The calculation of such defects is a problem in lattice dynamics and requires a knowledge of local modes of vibrations of the perfect crystal and precise nature of the defects. Localized modes of vibration occur when the defect consists of an impurity atom which is some what lighter than the atoms of the host crystal, provided the force constants between this atom and its neighbours have a similar strength to those between pairs of the host crystal atoms. To study these localized vibrational modes, infrared spectroscopic technique is used. The resulting infrared spectrum represents the fingerprint of the sample and the absorption peaks in the spectrum represent the frequencies of vibrations of the atoms of the sample. So IR spectroscopy is a very useful technique for the analysis of materials.

1.5 Motivation Of This Project

The prime motivation behind this work is to study the local vibrational modes (LVM) in silicon using FTIR technique. These local vibrational modes arise due to the presence of impurities in the material. In silicon, the most common impurities are carbon and oxygen. These impurities are unintentional impurities and arise during crystal growth. Carbon occupies normal substitutional sites, where as oxygen occupies interstitial as well as substitutional sites in the silicon lattice. These impurities have well known absorption bands at 605 cm^{-1} and 1107 cm^{-1} respectively at room temperature.

We used FTIR Spectroscopy to study the defects in Si. We studied different samples of Si which were prepared by Czochralski technique as well as Floating-zone technique. The Fourier transform infrared (FTIR) is an optical technique. This technique is preferred over older techniques for several reasons:

- It is a non-destructive technique.

- It provides a precise measurement method which requires no external calibration.

- It can increase speed, i.e., collecting a scan every second.

- It can increase sensitivity, i.e., one second scans can be co-added to ratio out random noise

- It has greater optical throughput.

- It is mechanically simple with only one moving part [3].

CHAPTER NO 2

THEORY OF FOURIER TRANSFORM INFRARED (FTIR) SPECTROSCOPY

There are two extremes in the attitudes of the research scientists towards the new instrumentation. These extremes might apply to the acquisition of an FTIR spectrometer. On the one hand is the attitude of the extreme optimist. On the other hand is the attitude of the extreme pessimist. " I know that the new instrument will offer some advantages, but no instrument is perfect; there will be a whole new set of annoying problems and breakdowns about which the salesman will not forewarn me which I will not be equipped to handle." Neither of these two extreme attitudes properly applies to an FTIR spectrometer [7].

The original infrared instruments were of despercive type. These instruments separated the individual frequencies of energy emitted from the infrared source. This dispersion was accomplished by the use of a prism or grating.

The principles of Fourier transform infrared spectroscopy are different from those of dispersion spectroscopy. The principal advantage of Fourier transform spectroscopy over the conventional spectroscopy is its higher signal- to- noise ratio [8]. An FTIR spectrometer basically consists of two parts; (1) an optical system which uses an interferometer and (2) a dedicated computer. The computer controls the optical components, collects and stores data, performs computations on data, and displays the spectra. Thus the real advantages of an FTIR spectrometer result from the use of an interferometer rather than a grating or prism.

Major distinctions between FTIR spectrometers are based on the design of the interferometer and the manner in which the interferometer is operated. It may be operated by scanning in a discontinuous, stepwise manner (Step scan interferometer), a slow continuous manner with chopping of infrared beam (slow scanning, or rapid scanning). We will describe here the rapid scanning Fourier transform spectrometer with a Michelson interferometer, because this type of instrument seems to have emerged as the most practical form of FTIR spectrometer for widespread application to the chemical problems in all regions of the infrared spectrum [7].

2.1 Optics of Fourier Transform Infrared Spectrometer

A schematic diagram of the essential components of a rapid scanning Fourier transform spectrometer is shown in Fig. 2.1. An FTIR spectrometer basically consists of a Michelson interferometer. Michelson interferometer consists of five parts, (1) IR source, (2) Beam splitter, (3) Fixed mirror, (4) Moving mirror, (5) Detector. The light from the infrared source is collimated and sent to the beam splitter of a Michelson interferometer. The beam is divided by the beam splitter, one part goes to the moving mirror and second part to the fixed mirror. The returning beams recombine at the beam splitter undergoing interference. The reconstructed beam is then directed through the sample and focused onto the detector. The motion of the moving mirror results in a signal at the dector which for a given wavelength (λ) varies sinusoidally with a frequency $\omega = Vm/\lambda$ (or $\omega = Vm\ \bar{\nu}$), where Vm is the velocity of the moving mirror.

A laser beam, undergoing the same change of optical path as the infrared beam, serves to reference the position of the mirror during the scan and initiates the

collection of data points from the signal of the infrared detector at uniform intervals of mirror travel. The data points are digitized by an analog- to - digital converter and stored in a computer memory. The result is an interferogram, i. e., a record of the signal of the infrared detector as a function of optical path difference (retardation) for the two beams in the interferometer. The interferometer scans are generally taken quite rapidly (a few seconds each). Data from additional scans can be coadded to the data stored in computer memory to improve the signal- to-noise ratio of the interferogram.

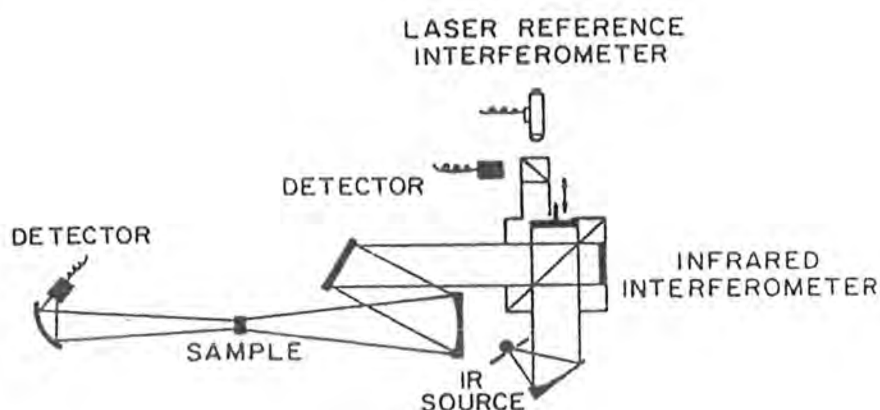

Fig. 2.1 Simplified diagram of the optical system of a Fourier transform infrared spectrometer.

The averaged interferogram is prepared for computation by phase correction and apodization and a Fourier transformation is performed on the interferogram using a fast Fourier transform algorithm:

$$S(\nu) = 2\int_0^\infty I(x)\cos(2\pi\nu x)dx$$

The Fourier transform converts the signal as a function of retardation (i. e., the interferogram I(x)) to a signal as a function of frequency [i. e., the spectrum S(ν)].

We can write:

$$I(x) = 2\int_{0}^{\infty} S(\nu)\cos(2\pi\nu x)d\nu$$

I(x) is called an interferogram function; i. e., the intensity as a function of distance. Fig. 2.2 shows a scheme of an interferogram. We notice that I(x) has positive and negative values. It is a convenient function for the calculation of the Fourier transform S(ν) which gives us the desired intensity - frequency distribution.

Fig. 2.2 Interferogram

Considering S(ν) to be an even function in the entire frequency range, we can write the following pair of Fourier transform.

$$I(x) = \int_{-\infty}^{+\infty} S(\nu)\cos(2\pi\nu x)d\nu \qquad \ldots(1)$$

and,

$$S(\nu) = \int_{-\infty}^{+\infty} I(x)\cos(2\pi\nu x)dx \qquad \ldots(2)$$

Equation (2) is the Fourier transform of equation (1)

For both even and functions, the above equations can be written as

$$I(x)=\int_{-\infty}^{+\infty} S(\nu)\exp[i2\pi\nu x]\, d\nu \text{------------}(a)$$

and,

$$S(\nu) = \int_{-\infty}^{+\infty} I(x)\exp[-\imath 2\pi \nu x]\,dx \text{---------}(b)$$

2.2 Apodization:

In the previous section we used the limits of x between -∞ and +∞. In reality, x is restricted to $-L \le x \le L$, where L is the distance which the moving mirror travels. This finite movement of the mirror can be expressed by multiplying I(x) in equation 1 with a symmetric 'window function'

$$P(x) = \begin{bmatrix} 1 & \textit{for } -L \le x \le L \\ 0 & \text{for all other values of x} \end{bmatrix} \qquad \ldots(3)$$

With this function we can calculate an approximate value of the integral in equation 2.

Now $$S_I(\nu) = \int_{-\infty}^{+\infty} I(x)P(x)\cos(2\pi\nu x)dx \qquad \ldots(4)$$

$S_I(\nu)$ is the Fourier transform of the product of I(x) and P(x). This Fourier transform $S_I(\nu)$ can be expressed by using the convolution theorem which states; the Fourier transform of the product of the two functions I(x) and P(x) is equal to the convolution of the Fourier transform of I(x) and P(x).

i.e., $$S_I(\nu) = \int_{-\infty}^{+\infty} g(\tau)\phi(\nu-\tau)d\tau \qquad \ldots(5)$$

Where

$$g(\tau) = \int_{-\infty}^{+\infty} I(x)\cos(2\pi\tau x)dx \qquad \ldots(6)$$

and

$$\phi(\tau) = \int_{-\infty}^{+\infty} P(x)\cos(2\pi\tau x)dx \qquad \ldots(7)$$

The integral in equation (7) is easily computed with the help of equation (3).

So we have,

$$\phi(\tau) = 2L\frac{\sin(2\pi\tau L)}{(2\pi\tau L)} \quad \ldots(8)$$

The function Sin(Y)/Y is sometimes designated by SincY.

Now substituting equation 8 in equation 5, we get.

$$S_1(\nu) = \int_{-\infty}^{+\infty} g(\tau)2L\frac{\sin[2\pi(\nu-\tau)L]}{[2\pi(\nu-\tau)L]}d\tau \quad \ldots(9)$$

0r,

$$S_1(\nu) = \int_0^{\infty} g(\tau)2L\left\{\frac{\sin[2\pi(\nu-\tau)L]}{[2\pi(\nu-\tau)L]} + \frac{\sin[2\pi(\nu+\tau)L]}{[2\pi(\nu+\tau)L]}d\tau\right\} \quad \ldots(10)$$

The equation 9 0r 10 is interpreted as the convolution of the actual spectrum S(ν) with the " Theoretical apparatus function".

$$A_p(\nu,\tau) = 2L\{\sin c[2\pi(\nu-\tau)L] + \sin c[2\pi(\nu+\tau)L]\} \quad \ldots(11)$$

For the simple example of a monochromatic input, the output for finite path differences is represented by.

$$\acute{A}_p(\nu,\nu_o) = 2L\{\sin c[2\pi(\nu-\nu_o)L] + \sin c[2\pi(\nu+\nu_o)L]\} \quad \ldots(12)$$

The quantity $A'_p(\nu, \nu_0)$ has the appearance of the Sinc- function with two peaks centred at $\nu = +\nu_0$ and $\nu = -\nu_0$. The peaks at $-\nu_0$ and $+\nu_0$ have wings; therefore we can neglect here the peak at $-\nu_0$ as we did in the case of δ- function. Now neglecting the second term in equation (12), we have

$$\acute{A}''_{p_1} = 2L\sin c[2\pi(\nu-\nu_o)] \quad \ldots(13)$$

This equation can be plotted in Fig. 2.3

The side lobes of the function A''_{p1} arise from the abrupt termination of the interferogram at x= L through P(x). These side lobes, some of them negative, may cause distortion in the analyzed spectrum. Removing or suppressing them can be

accomplished by replacing the window function P(x) by other functions. This process is called "apodization". The following two apodization function are frequently used.

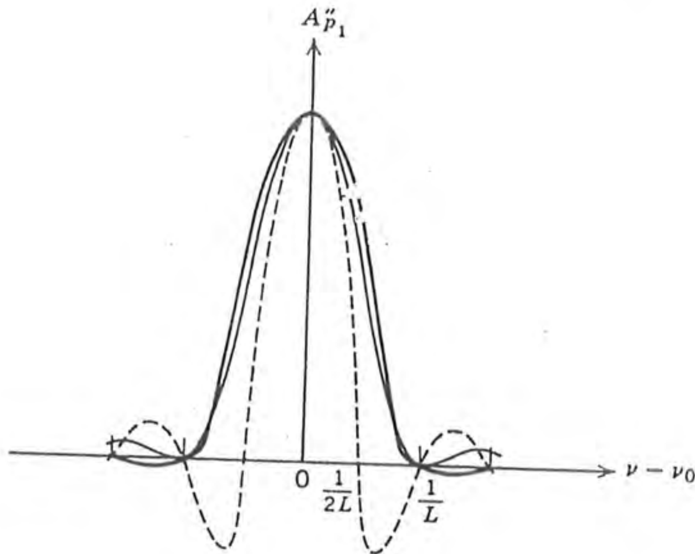

Fig: 2.3 Theoretical apparatus function.

$$\text{(1)} \quad h_1(x) = \begin{bmatrix} (1-\left|\frac{x}{L}\right|) & \textit{for } -L \leq x \leq L \\ 0 & \text{for all other values of x} \end{bmatrix} \qquad \ldots(14)$$

The second apodization function is.

$$\text{(2)} \quad h_2(x) = \begin{bmatrix} (1-\frac{x^2}{L^2}) & \textit{for } -L \leq x \leq L \\ 0 & \text{for all other values of x} \end{bmatrix} \qquad \ldots(15)$$

These apodization functions are shown in Fig. 2.4

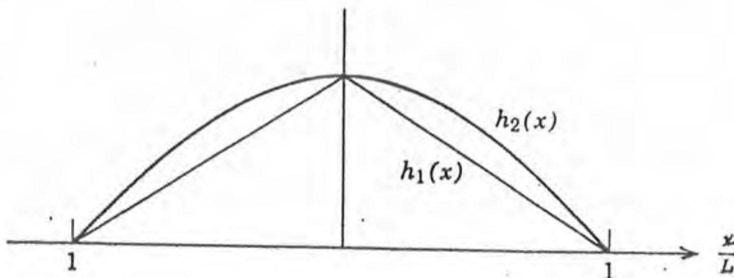

Fig: 2.4 Plot of $h_1(x)$ and $h_2(x)$ as a function of x/L

By using these functions, the sides wings are considerably smaller than in the case of the window function P(x). As a consequence, the spectrum will be smoother. Apodization is effective if information about unresolved or poorly resolved bands is required [8]. In our FTIR spectrometer, two apodization functions are available, i.e, Happ- Genzel (HG) and Boxcar (BX) functions. In our measurements we have used Happ- Genzel (HG) function as an apodization function.

2.3 Resolution

The spectral resolution of any spectrometer, whether despersive or interferometeric, is a function of the total optical retardation available, that is, the total path difference between waves at the extremes of the system. In a despersive spectrometer, this is proportional to the size of the diffraction grating, in an interferometric spectrometer, it is proportional tot he total travel of the moving. It is well known that Fourier-transform interferometric spectrometers have obtained higher spectral resolution than dispersive spectrometers, achieving resolutions of the order of 0.002 cm^{-1}, corresponding to a mirror travel of approximately 2m.

However, if one is only interested in the highest-resolution spectrometer one can buy off-the-shelf, it turns out that the very-long-travel interferometers are not available commercially, but, rather, have been made on a custom basis, generally by the user scientists themselves [9].

The spectral resolution obtained in Fourier spectroscopy is primarily determined by the maximum optical path difference attained during the interferogram

measurement. When no apodization is applied to the spectrum, the corresponding apparatus function is given by

$$A_p(\nu,\tau) = 2L\{\sin c[2\pi(\nu-\tau)L] + \sin c[2\pi(\nu+\tau)L]\} \qquad \ldots(1)$$

Wheere 'L' is the maximum path difference. If the inteferogram is tapered by triangular function given by

$$h_1(x) = \begin{bmatrix} (1-|\frac{x}{L}|) & for\ -L\leq x\leq L \\ 0 & \text{for all other values of x} \end{bmatrix} \qquad \ldots(2)$$

The apparatus function $A_p(\nu, \tau)$ becomes

$$A_p(\nu,\tau) = L\sin c^2[\pi(\nu-\tau)L] \qquad \ldots(3)$$

In practice the interferogram processing is done by multiplying the interferogram by the triangular function $h_1(x)$ intended to accomplish (1) apodization of the sinc apparatus function and (2) reduction of the high frequency noise in the recovered spectrum. The resolution for such an apparatus function is often quoted as being (1/L), which corresponds to the full width at its half height. The spectrum even for this case, however, must be computed at every interval of (1/2L) [9]. Thus the resolution will be improved by taking the larger and larger values for L.

2.4 Beam Splitters

Beam splitter is a very crucial part of the Michelson interferometer. It is required to split the incident radiation into two equal parts. One goes toward the moving mirror and the other goes toward the fixed mirror. Many of the optical instruments, such as the Michelson and Troyman-Green interferometers, range finders and optical gunsights, utilize beam splitters. The conventional beam splitter which

consists of a thin film of silver, has the disadvantage that it not only rapidly deteriorates in quality but also is inefficient because it absorbs approximately one-third of the incident flux. Multilayer beam splitters do not deteriorate and are composed of dielectric films which absorb a negligible portion of the incident light. Multilayer beam splitters can have a neutral or a strongly peaked spectral transmittance. The latter type is called a "dichroic mirror" and is widely used as a color separator in television and photographic systems [10].

The beam splitter is the weakest point in the Michelson interferometer if a spectrum extending over one octave or more is to be studied. An ideal beam splitter requires T=R=0.5, where T is the transmissivity and R the reflectivity. The quantity 4RT may be used as an indicator of the efficiency of the beam splitter. In the ideal case the efficiency is unity. [8]. The wavelength region of the beam splitter is determined by the index of refraction and film thickness of beam splitter material. The relative efficiency of a beam splitter covers only the certain range of wave numbers. In the region 400-4000 cm^{-1}, germanium film beam splitters on various transparent are used. In our FTIR system a germanium coated KBr beam splitter is being used.

2.5 Advantages of Fourier Transform Infrared Spectroscopy

Fourier transform infrared spectroscopy offers potential advantages compared with conventional dispersion infrared spectroscopy, such as (1) higher signal-to-noise ratios for spectra obtained under conditions of equal measurement time, and (2) higher accuracy in frequency for spectra taken over a wide range of frequencies. The signal-to-noise advantage is a consequence both of the concurrent measurement of the detector signal for all resolution elements of the spectrum (multiplex advantage or Fellgett's advantage) and of the high optical throughout of the FTIR spectrometer

(throughout advantage or Jacquinot's advantage). The improvement in frequency accuracy of the FTIR spectrometer is a consequence of the use of a laser which references the measurements made by the interferometer (laser reference advantage or Connes advantage). These advantages are discussed below.

1. Throughput Advantage

One advantage of an FTIR spectrometer is the improved signal-to-noise ratio achievable as a consequence of the large optical throughput of the interferometer relative to that of a grating. The throughput E is defined as the product AΩ of the cross-sectional area and solid angle of the beam at any focus in the optical system. The maximum throughput of the optical system of the spectrometer also determines the maximum useful A Ω of the source. For a source of a given brightness, AΩ determines the total radiant power accepted by the optical system. It is desirable, therefore, to maximize the throughput (and, hence, the energy reaching the detector) so that the signal-to-noise ratio is maximized.

Thus, although an FTIR spectrometer has a theoretical throughput advantage over a grating spectrometer, the numerical value of the resultant signal-to-noise improvement is dependent upon several conditions. In favorable cases, an improvement results and this improvement may be used either to effect a time savings or to improve the quality of the spectrum [7].

2. Multiplex Advantage

Because all of the frequencies are measured simultaneously, most measurements by FTIR are made in a matter of seconds rather than several minutes. This is sometimes referred to as the Felgett Advantage or multiplex advantage.

The principal advantage of Fourier transform spectroscopy is a consequence of the fact that the interferogram contains information about all spectral elements (Fellgett or multiplex advantage). Let us designate the number of the spectral elements by N. Each particular spectral element is therefore studied for the total time T which is required to record the interferogram. In a grating spectrometer in contrast, one studies each spectral element only during the time interval T/N, thereafter switching to the next spectral element [8].

Because the signal-to-noise ratio improves as the square root of the observation time of each resolution element $\Delta\nu$, interferometer system offers a signal to noise advantage. This improvement in the signal-to-noise ratio is achieved only if (1) the noise in the spectrum is due to the detector noise and (2) the detector noise is not proportional to the detector signal. So it is the multiplex advantage which represents the principal advantage of FTIR spectrometers over grating spectrometers.

3. Laser Reference Advantage

An FTIR spectrometer determines frequencies by direct comparison with a visible laser output. Potentially this offers an improvement in frequency accuracy which is sometimes called the "connes advantage". It has been reported [7] that the use of a laser reference represents a major advantage of FTIR spectrometers over grating

spectrometers. FTIR spectrometer uses HeNe laser as an internal wavelength calibration standard (referred to as connes advantage). These instruments are self-calibrating and never need to be calibrated by the user.

In addition to these optical advantages, the Fourier transform spectrometers have very important data processing advantages. The computer used to do the Fourier transform is also used in manipulating and displaying the spectra. The ability to add and subtract spectra in digital form is especially useful in eliminating interferences due to overlapping bands. This allows one to extract a maximum amount of the information available in the spectrum.

2.6 Applications of FTIR Spectroscopy

FTIR stands for Fourier Transform Infrared, the preferred method of infrared spectroscopy. Infrared spectroscopy has been a work horse technique for materials analysis in the laboratory for over seventy years. In infrared spectroscopy, IR radiation is passed through a sample. Some of the infrared radiation is absorbed by the sample and some of it is passed through (transmitted). The resulting spectrum represents the molecular absorption and transmission, creating a molecular fingerprint of the sample. No two unique molecular structures have the same infrared spectrum. This makes infrared spectroscopy useful for several types of analysis.

There are many applications of FTIR spectroscopy. Some of them are mentioned below:

- Chemical analysis of a wide range of solids, liquids and gases.

- Determination of the infrared optical properties of solids, liquids and gases.
- Determination of epitaxial silicon layer thickness.
- Surface analysis, including detection and monitoring of monolayers.
- Analysis of silicon cleaning process.
- Characterization of novel and oxynitride thin films using photo-assisted deposition process.
- Analysis of gaseous components of out gasses material in conjunction with thermal Gravimetric Analysis.
- In-situ monitoring tool of materials by emission-FTIR

In addition to these applications, FTIR also provides the following information.

- It can identify unknown materials.
- It can determine the quality or consistency of a sample.
- It can determine the amount of components in a mixture.
- It can give the covalent-bond energy of various vibrational modes [11].

CHAPTER 3

EXPERIMENTAL DETAILS

This chapter describes the details of the experimental set up and the procedure for the data collection of the FTIR absorption spectra of silicon samples.

3.1 Samples

The material used in this study was silicon (Si) crystals. We studied two different sets of Si samples grown by using two different growth techniques, the Czochralski (CZ) growth technique and the Floating-zone (FZ) technique. Both these techniques are described below:

3.1.1 Czochralski Crystal Growth Technique

The success in fabricating very large-scale integrated (VLSI) circuits is a result of the development in the growth of pure single-crystal semiconductor materials. The high purity means that extreme care is necessary in the growth and fabrication processes. The mechanics and kinetics of crystal growth are extremely complex and are described in only very general terms. However, a general knowledge of the growth techniques is valuable.

A common technique for growing single-crystal materials is called the Czochrolski method. In this technique, a small piece of single-crystal material, known as a seed, is brought into contact with the surface of the same material in liquid phase, and then slowly pulled from the melt. As the seed is slowly pulled, solidification occurs along the plane between the solid-liquid interface. Usually the crystal is also

rotated slowly as it is being pulled, to provide a slight stirring action to the melt, resulting in a more uniform temperature. A schematic of CZ-growth is shown in Fig. 3.1 [12].

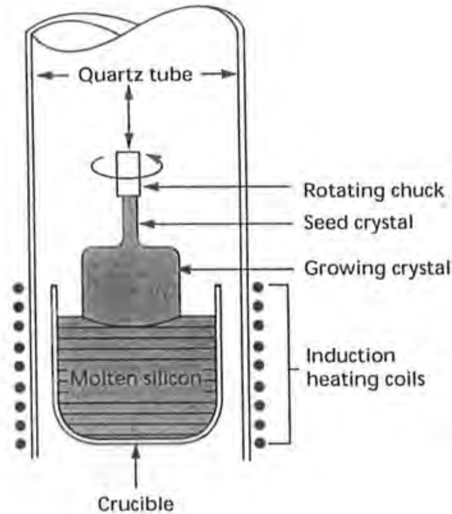

Fig. 3.1 Schematic illustration of the Czochralski technique.

The two important differences from other melt-growth processes are that the liquid-solid interface is not in contact with the crucible and, although a crucible is used to hold the melt, it does not act as a mould. The lack of any restraint by a mould is advantageous and can result in pulled crystal having a high degree of crystal perfection. Sworn and Brown have grown dislocation-free copper crystals by Czochralski technique, and dislocation-free aluminium, germanium and silicon crystals have also been grown by this method. The crystals resulting from Czochralski pulling approximate to a circular cross-section and diameter of the crystal depends primarily on the melt-temperature and the pulling rate. For a given melt-temperature, the crystal diameter decreases as the pulling rate increases and for a fixed pulling

rate, the crystal diameter decreases as the melt-temperature increases. This method is capable of producing excellent crystals but requires precise control over the growth rate and particularly temperature. It is usually possible to arrange some mechanical system to give a constant pulling rate to the seed crystal holder [13].

In this technique both oxygen and carbon arise unintentionally during the growth process. Oxygen is in high concentration while carbon in somewhat lower concentration.

3.1.2 Float-Zone Technique

Impurities can be present in the CZ-grown crystals. Zone refining is a common technique for purifying materials. One such technique is a floating-zone technique. This technique was originally developed by Kech and Golay and used by others for the preparation of high purity silicon.

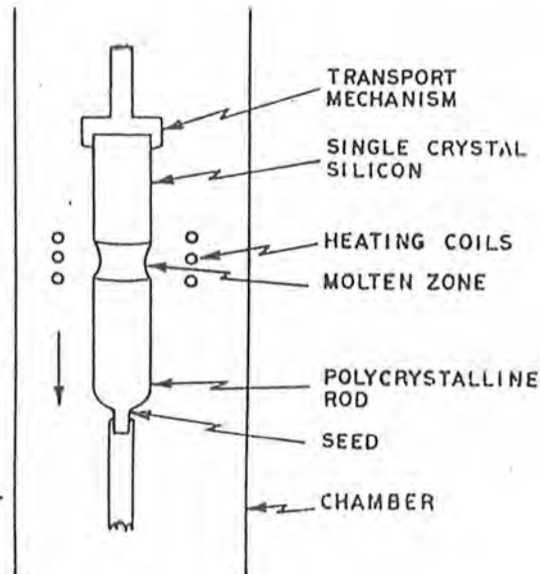

Fig. 3.2 Schematic illustration of the Float-zone technique.

The basic idea is illustrated in Fig.3.2. In this treatment only a part of the material is melted at a given instant, and in essence, a liquid zone is moved along a length of a (long) solid charge rod. The rod is typically 100-150 mm in length and 3-6 mm in diameter, mounted vertically and held at both ends. The charged rod is encircled by a heat-source focused to give a narrow molten zone, and the molten zone is held in place by surface tension effects.

The movement of the heat source, as indicated in Fig.3.2, moves the molten-zone from end to end of the charge rod. The shape, size and the stability of the molten-zone has been considered on a theoretical basis by Kech et al., and Heywany, in terms of rod radius, liquid density and surface tension etc. In practice it is found that for rods of up to ~6mm diameter a molten-zone length approximately equal to the rod diameter is suitable. In an exercise to increase molten-zone stability in iron, Oliver and Shaler passed a d.c. current along the length of the rod. This approach deserves more attention and could find possible application allied to purification by electro-transport mechanisms. The forms of heating used to obtain the molten-zone are varied, but electron bombardment and induction heating are by far the most common [13]. As the liquid zone moves through the material, the impurities are driven along with the liquid, and ultimately the impurities reach at the end of the bar, which can then be cut off. Thus the moving molten zone, or the zone-refining technique can result in considerable purification [1].

3.2 Experimental Set-Up

Our experimental set-up consists of the following systems:

1. Compressor-Dryer System
2. Fourier Transform Infrared (FTIR) Spectrometer System

1. Compressor-Dryer System

This system consists of four components.

(i) Compressor

General Electric Model: No. 7HDE-10-M701X

A Compressor is used to compress the air and sends it to the spectrometer at a pressure of 70-90 psi.

(ii) Dryer

General Cable Corporation, Model: No.P-05411-434

The dryer extracts carbon dioxide and absorbs water. It is a pure gas heatless dryer.

(iii) Filter

Deltech Filter Model: No.111

It removes oil and dust particles from the compressed air.

(iv) Air Pressure Regulators

C.A. Norgren Co. Model: Np.B07-102 M 1KA

It has two tubes, one tube is used to purge the whole system with air and the other tube sends air at a controlled pressure of 20-30 psi to the air bearings of movable mirror.

2. Fourier Transform Infrared (FTIR) Spectrometer System

Our FTIR spectrometer system consists of two basic components, (1) The Optical System, (2) The Data System.

1. The Optical System

The optical system is used to collect data. It essentially consists of an optical bench or spectrometer, which further consists of Michelson's Interferometer.

Michelson's Interferometer

The interferometer produces a unique type of signal which has all of the infrared frequencies encoded into it. Thus the resulting signal is an interferogram. An interferogram is obtained by the superposition of two light beams and the variation of their optical path difference.

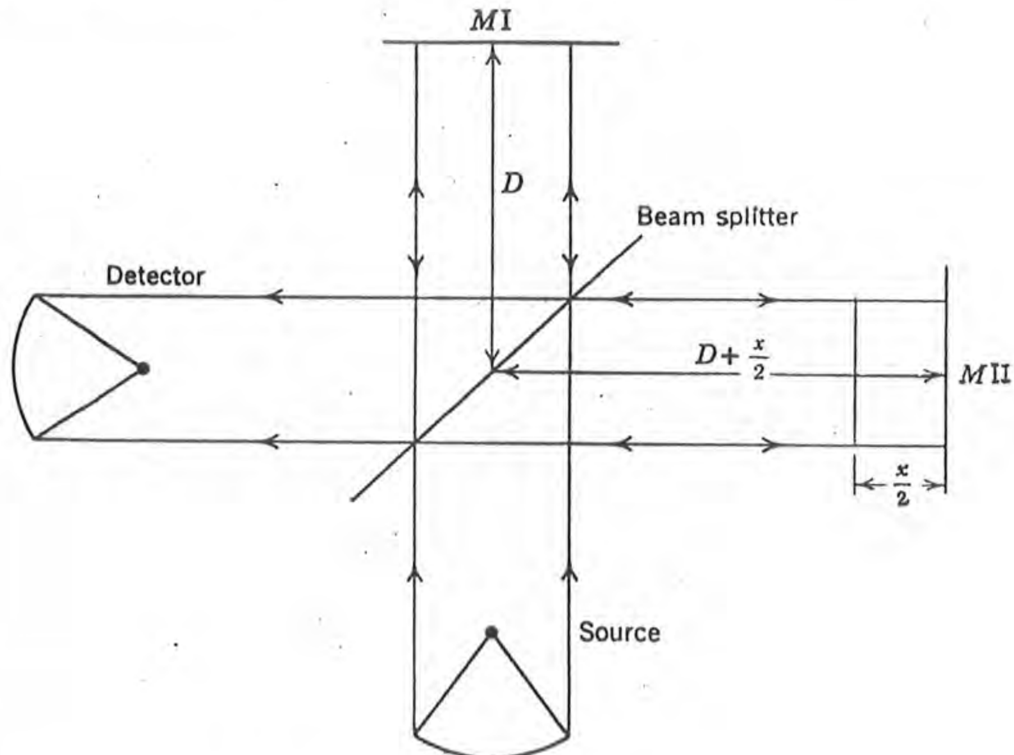

Fig. 3.3 Optical Schematic of a Michelson Interferometer

In particular, the interferogram is recorded in terms of the intensity as a function of distance, and by Fourier analysis converted into an intensity versus frequency distribution. This means that as the interferogram is measured, all the frequencies are being measured simultaneously. Thus, the use of the interferometer results in extremely fast measurements. The interferometer consists of five parts, such as source, beam splitter, a moving mirror, a fixed mirror and a detector. The schematics of Michelson interferometer are shown in the Fig.3.3.

a. Source

In our FTIR system, the source is a Globar. A Globar is a small rod of silicon carbide (SiC). The maximum radiation energy from the Globar occurs in the range of 5500 – 5000 cm^{-1} and drops off as the 600 cm^{-1} region is approached.

b. Beam Splitter

The beam splitter is used to split the incident radiation into two equal parts. One part goes towards the fixed mirror and the other goes towards the moving mirror. In our FTIR system a germanium coated KBr beam splitter is being used. This is effective in the wave numbers range between 400 – 4000 cm^{-1}.

c. Detector

We have used Triglycerine Sulfide (TGS) detector in our system. Detector is used to measure the radiation energy, which is incident at the detector.

d. Alignment Source

In our system HeNe laser (1mw) is used as an alignment source.

(2) The Data System

The data system consists of the following components:

- Nicolet's 1280 Computer (DXB).
- A Color display terminal (monitor).
- Key board.
- A plotter.

  Model No: 7470A; Serial No: 2644V 02075

The computer controls the optical components, collects and stores data, performs computations on data and displays spectra.

3.3 The Data Collection

To collect data from a sample, we first need to collect a background. This must always be done without the sample in the spectrometer.

3.3.1 Background Measurements

The reason of taking the background spectrum before the sample spectrum was that to avoid the features of water vapors and carbon dioxide (CO_2) which are present in background (dry air). Since while taking the sample data, we have a sample and background (dry air) data, so to get a real sample spectrum, the background must be subtracted from the sample. This was done automatically by a computer.

To collect background we proceed as follows:

Go to main menu.

1. Collect Data.
5. View/Change parameter (if necessary).
3. Collect Background.

Before collecting the background data, we have to change the necessary parameters by selecting 5-view/change parameter option. The background data was collected with the following parameters.

Resolution = 1cm^{-1}

Number of scans for background (NSB) = 200 – 500

Detector gain (1, 2, 4, 8) (GAN) = 1

Mirror velocity (10, 20, 30, 40)) (VEL) = 30

Apodization function (HG, BX) (AFN) = HG (Happ-Genzel).

Aperture (BL, FL, MD, SM) (APT) = BL.

After changing the necessary parameters, we select 3- the collect background item from the collect data menu. The spectrometer then begins to collect background scans. The spectrometer can collect only the given number of scans. In our background measurements, the number of scans for background was 200 – 500 and the resolution was 1 cm^{-1}. The background must be at the same resolution as the subsequent sample data. The number of scans should be comparable but need not be the same.

During data collection, the live interferogram is displayed. The interferograms are co-added and Fourier transformed by a dedicated computer. After Fourier transformation, the background is displayed as a single beam. It is best to collect a background prior to every sample, though collecting a background once an hour or once a day may be sufficient. If an accessory is being used, a new background should be collected with no sample in place. The background spectrum is always displayed in emittance. The background spectrum is the total instrument response as a function of frequency. It is also called a single beam or unratioed spectrum.

In our work, we have collected two sets of background spectra. One the background spectrum with no sample holder and the other with an accessory (sample holder) in the spectrometer compartment.

The background spectra without any accessory are shown in figures 3.4, 3.5, 3.6. It is seen that various features due to CO_2 and H_2O molecules are observed in our background spectra. The features due to CO_2 molecule are observed at 2350 cm^{-1} and at 668 cm^{-1}, and for H_2O molecule we have features at about 3700 cm^{-1} and at around 1500 cm^{-1}.

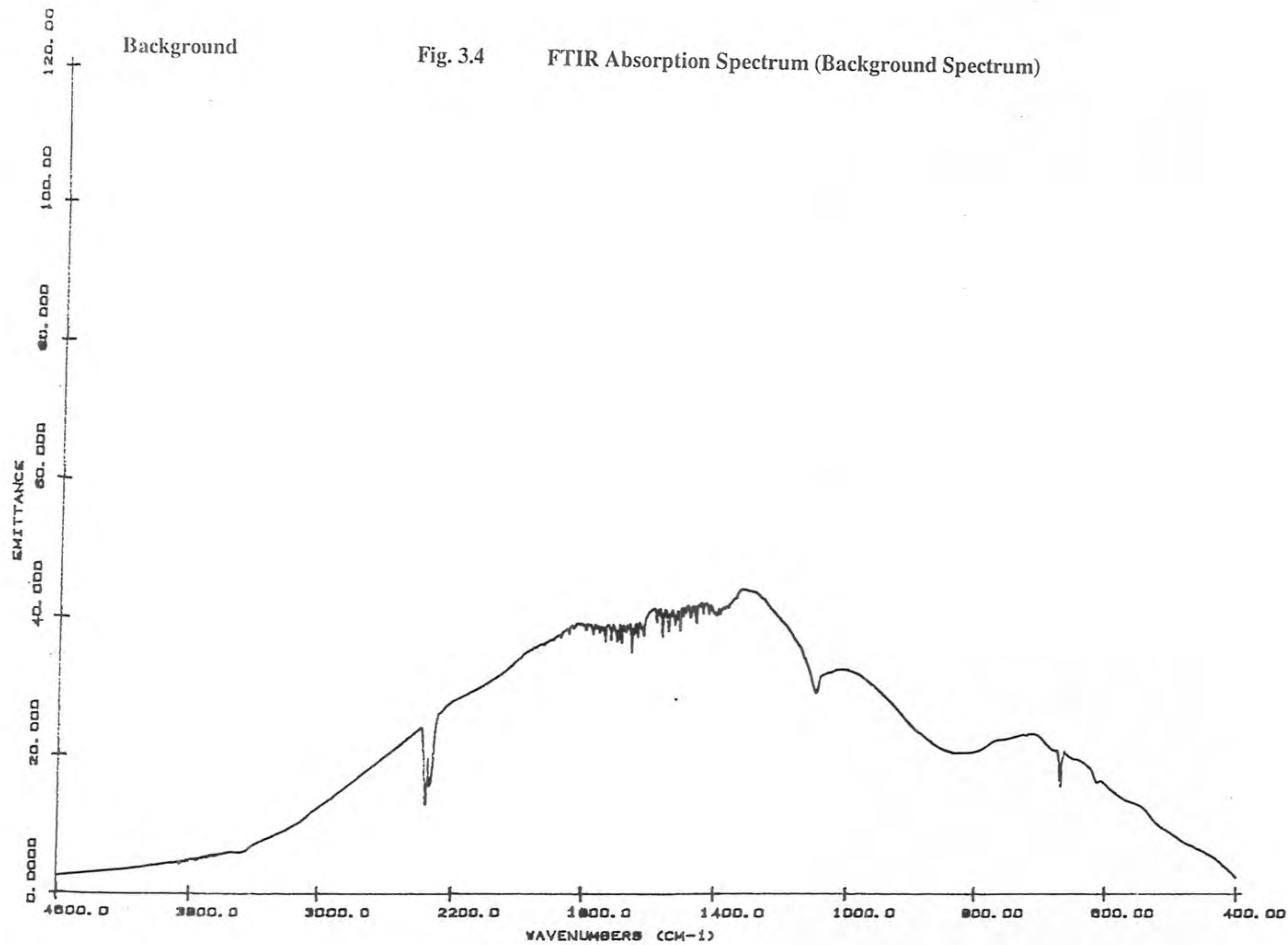

Fig. 3.4 FTIR Absorption Spectrum (Background Spectrum)

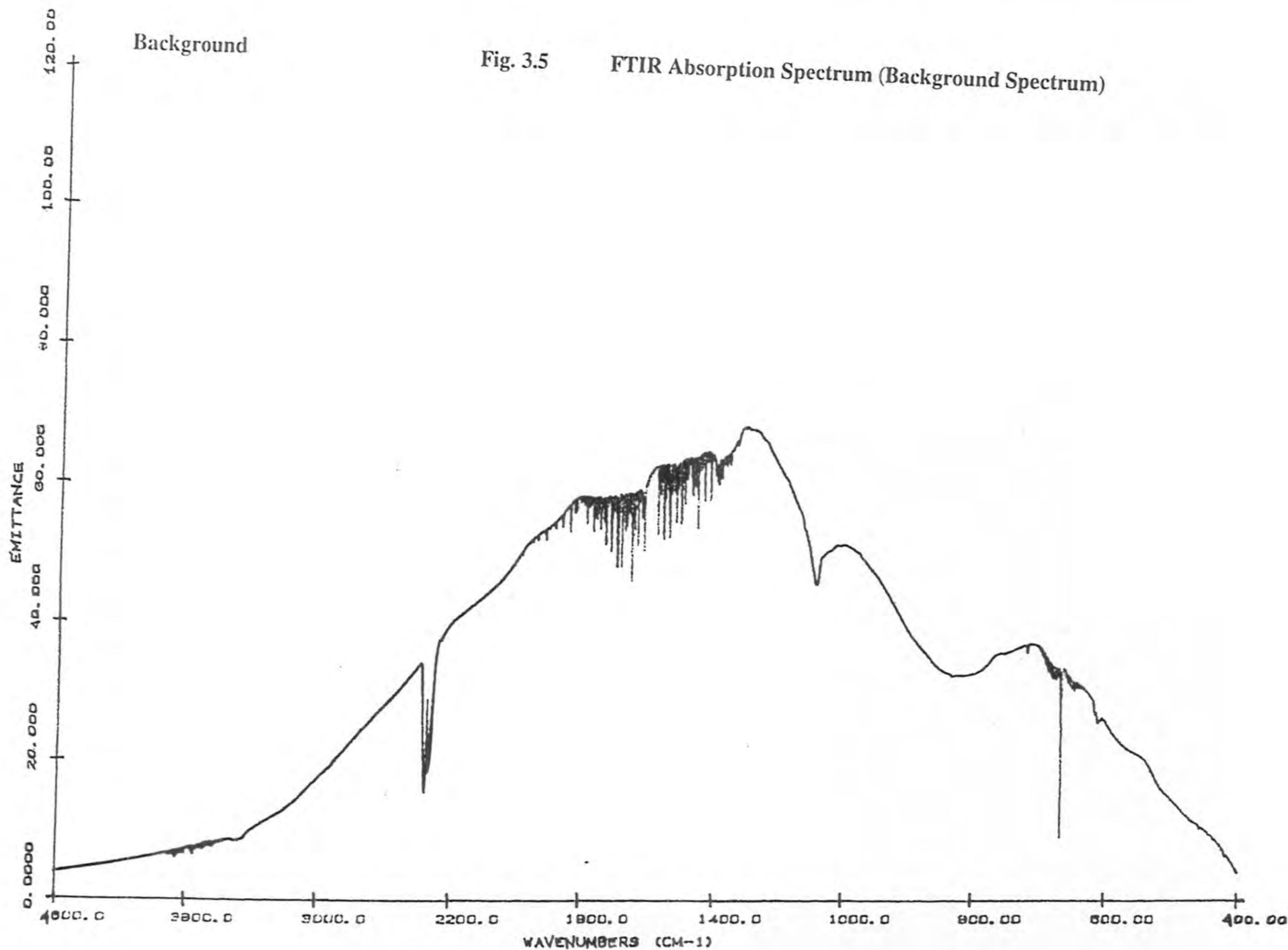

Fig. 3.5 FTIR Absorption Spectrum (Background Spectrum)

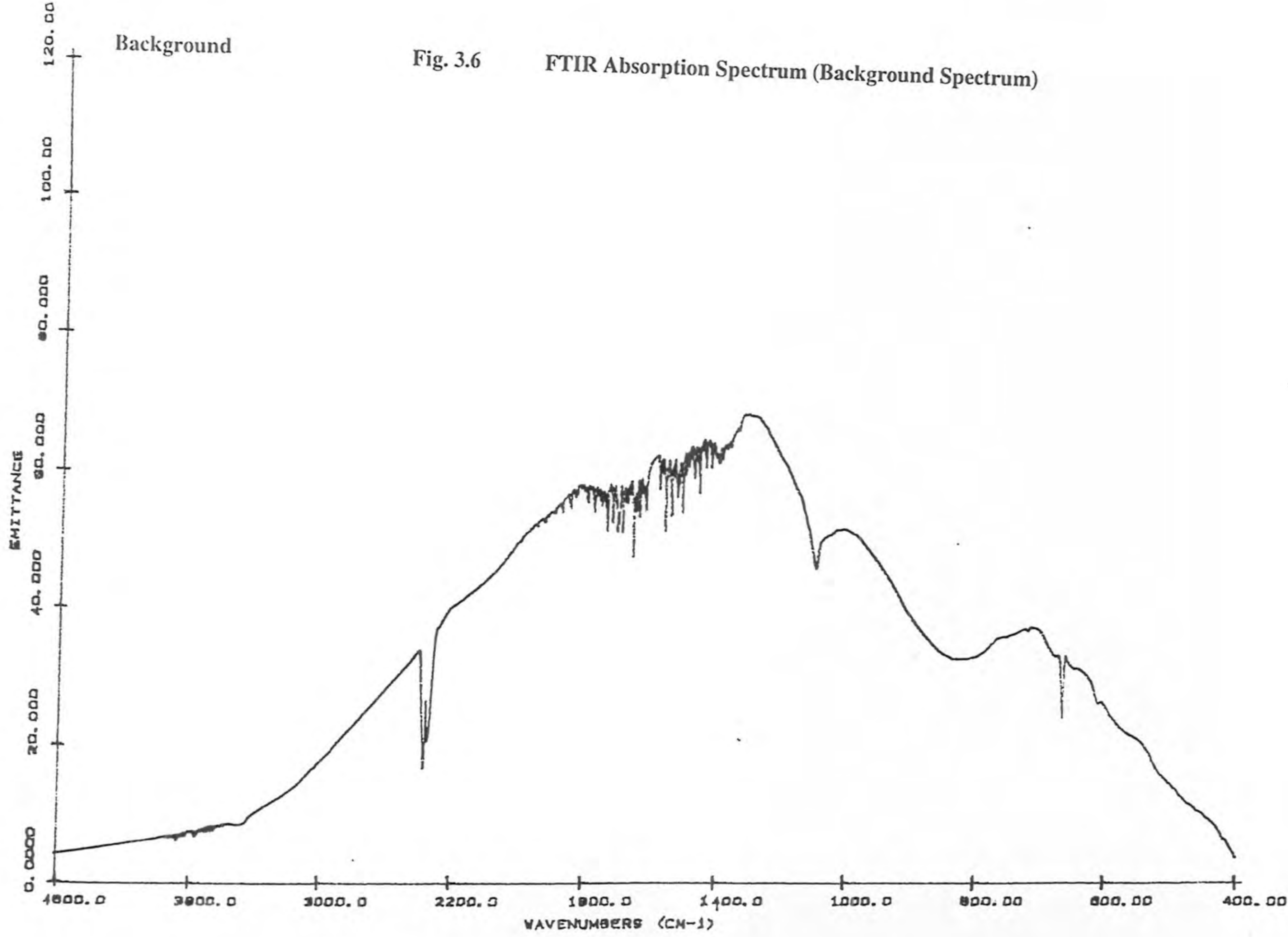

Fig. 3.6 FTIR Absorption Spectrum (Background Spectrum)

The Background Spectra with Sample Holder/Accessory

We obtained different background spectra with different accessories. Since, as we have mentioned above, if an accessory is being used a new background should be collected with no sample in place. This background was collected with the same parameters as mentioned above. These background spectra are shown in figures 3.7, 3.8, 3.9, 3.10 and 3.11.

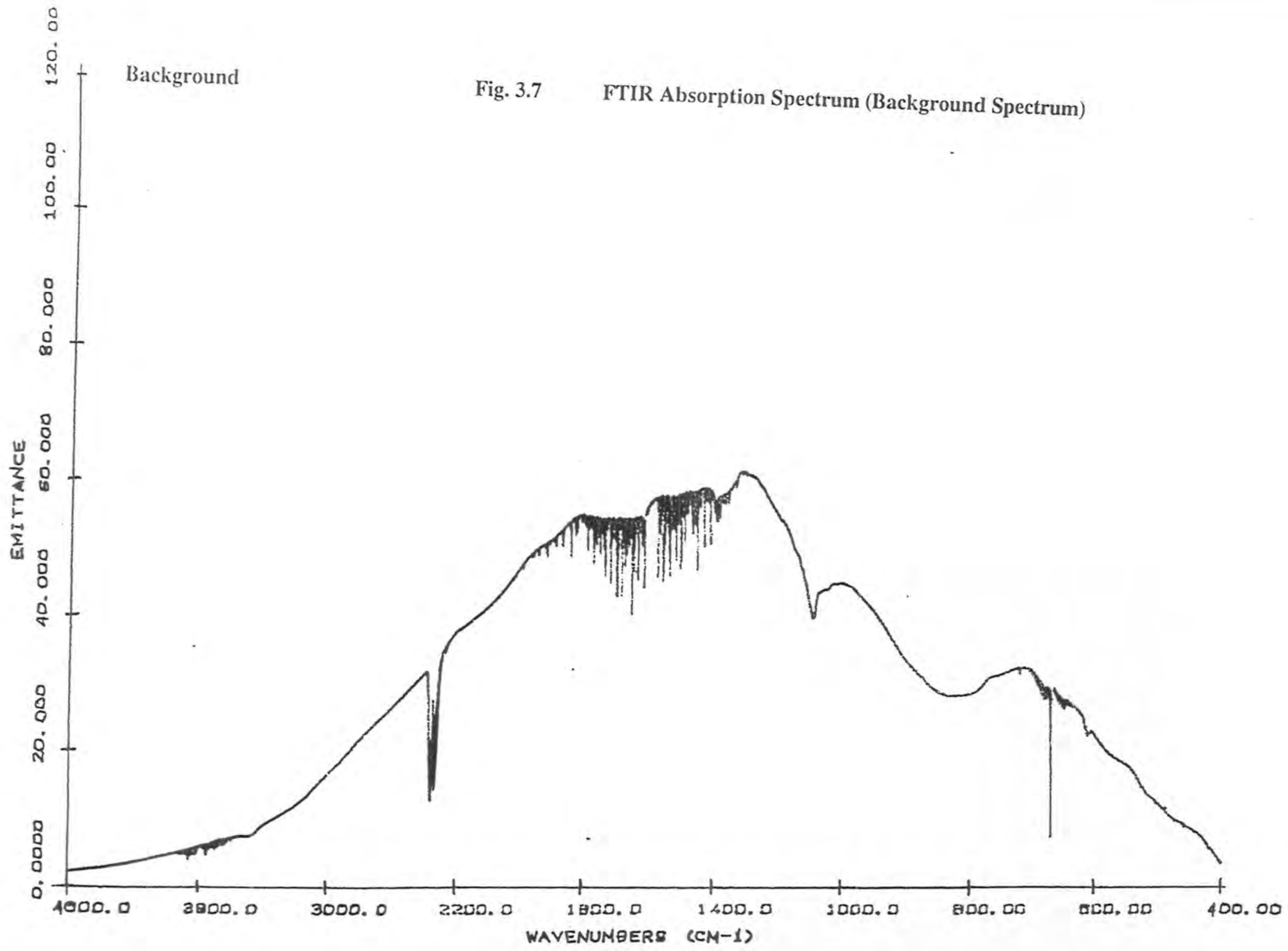

Fig. 3.7 FTIR Absorption Spectrum (Background Spectrum)

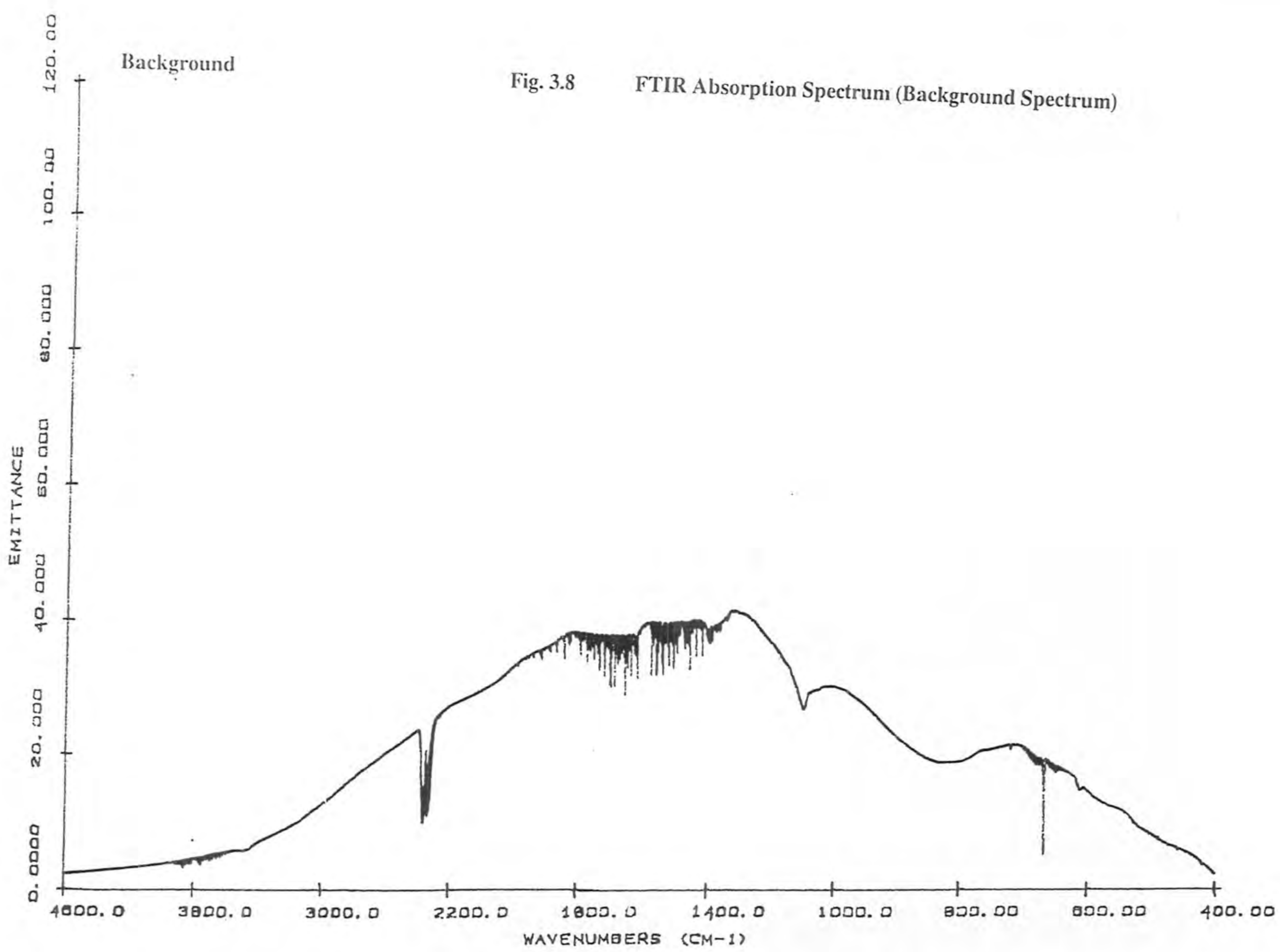

Fig. 3.8 FTIR Absorption Spectrum (Background Spectrum)

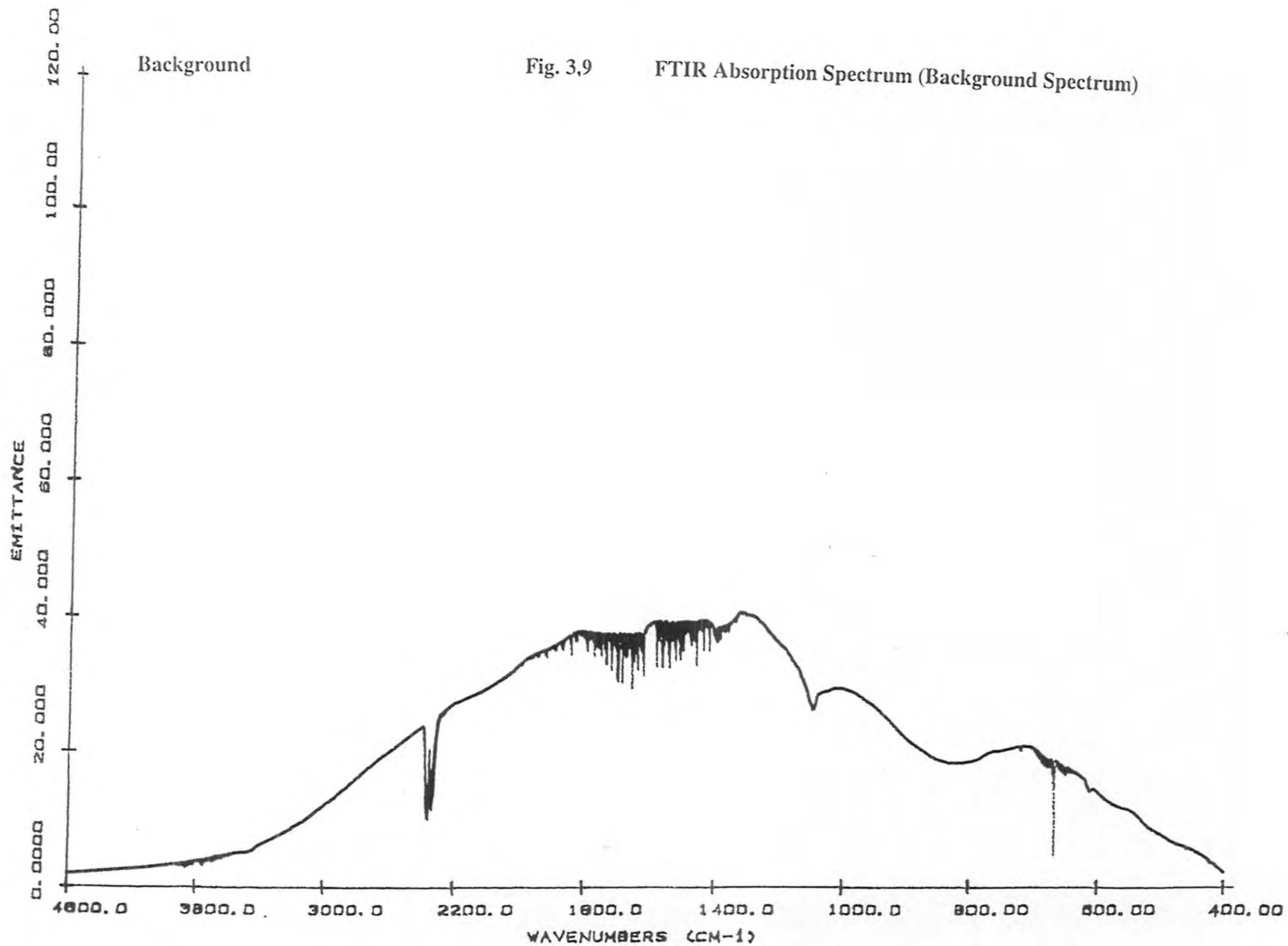

Fig. 3,9 FTIR Absorption Spectrum (Background Spectrum)

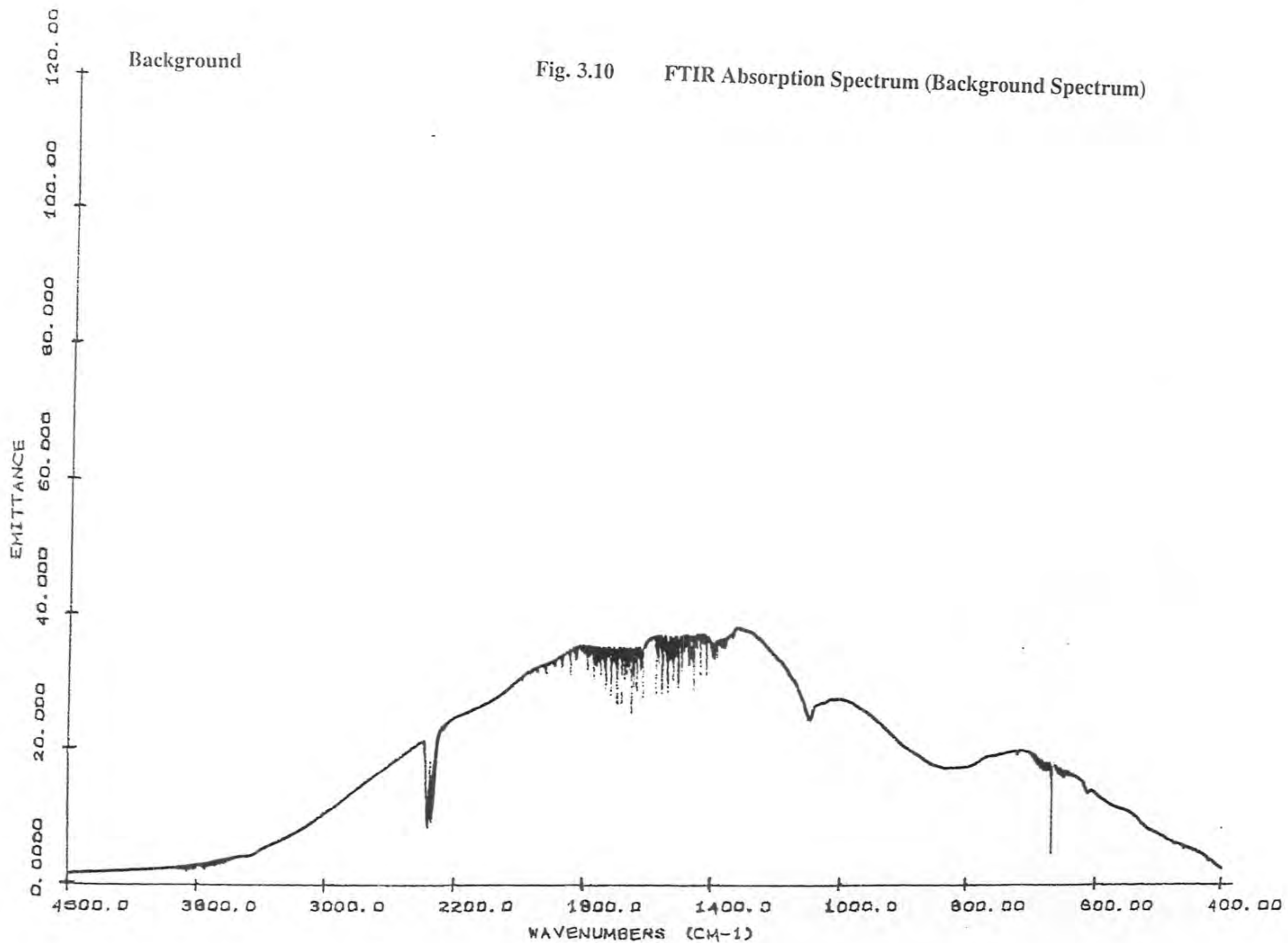

Fig. 3.10 FTIR Absorption Spectrum (Background Spectrum)

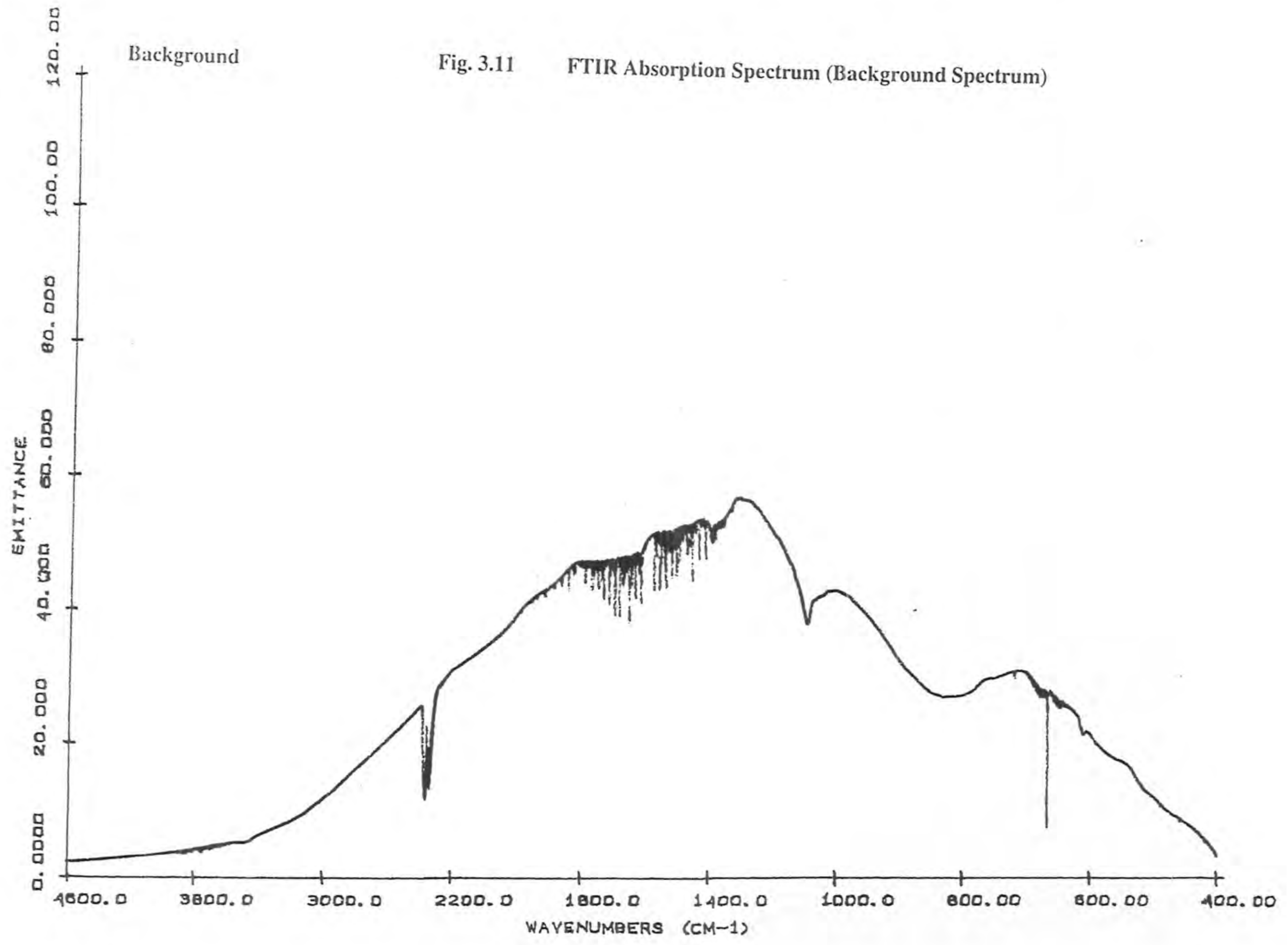

Fig. 3.11 FTIR Absorption Spectrum (Background Spectrum)

3.3.2 Sample Measurements

We have obtained the infrared absorption spectra of silicon samples in the wavenumber range 4600–400 cm^{-1} with the spectral resolution of 1 cm^{-1}. We took several measurements for different samples; all the measurements were performed at room temperature. The detail of collection of data is described below.

After the background has been collected, we inserted the sample into the spectrometer in the sample compartment and waited for a few seconds for the detector to stabilize. To collect data from the samples, we use a computer DXFTIR program with the following parameters.

(i) Resolution

The desired resolution for the spectrum can be selected before the collection of data. There is an option of 1 cm^{-1} 2 cm^{-1}, 4 cm^{-1}, 8 cm^{-1}, and 32 cm^{-1} resolutions in our system. The lower numbers mean the higher resolution. Both the sample and the background must be at the same resolution. For our work we have selected 1 cm^{-1} resolution for all the spectra.

(ii) Detector Gain

In our system the maximum value for the gain is 8, and the default value is 1. We have the options of 1, 2, 4 and 8 for the detector gain in our system. For the transparent or high throughput samples the detector gain of 1 is enough but for the low throughput samples the detector gain can be increased to higher values. We have used different values of gain for different samples. For high throughput samples, a

detector gain of 1 is used and for low throughput samples higher values of gain have been used.

(iii) Mirror Velocity

The mirror velocity can be optimized according to the type of the detector. For MCT detector the mirror velocity is 40 and for TGS detector the mirror velocity is 30. In our FTIR system the detector is TGS (triglycerine sulfied) and we have used 30 mirror velocity.

(iv) Number of Scans

An FTIR spectrometer requires only a one scan for a complete spectrum, the signal-to-noise ratio is improved by a factor proportional to the square root of the number of scans taken. The default value, for the number of scans in our system is 10, which can be changed to any value. It important to collect the comparable number of scans for background as well as sample. We have used 500 scans for the collection of data from the samples.

(v) Apodization Function

There is a provision of two apodization functions in our FTIR system, such as Happ-Genzel (HG) and the Boxcar (BX) functions. Normal data collection is accomplished with the Happ-Genzel (HG) apodization function. We have used Happ-Ganzel (HG) apodization function in our work.

As long as the data is being collected, the live interferogram is displayed. Whenever the size of the interferogram peak taken for the sample is less than 50% the

size of the open beam interferogram, the gain should be increased by a power of two until it is comparable to the open beam signal. The interferogram could not provide useful information. For this reason it is Fourier transferred by a computer to get a meaningful spectrum. We can display the spectrum in either emittance, % transmittance or absorbance, depending upon the display format selected from the display data menu item number 5- view/change parameters. These three display modes are described below.

(i) Emittance

The total instrument response is given in emittance. The background is always displayed in emittance. It is also called sigle beam or unrationed spectrum. The sample can also be displayed in this mode. The default value for y-axis is 0 to 120.

(ii) Transmittance

The ratio of the single beam spectrum of sample or reference to the background results in % transmittance spectrum. The mathematical operation is given by

$$\%T = 100\,(X/B).$$

Where 'X' is the single beam spectrum of sample or reference and 'B' in the background spectrum. The % transmittance scale is from 0 to 120.

(iii) Absorbance

The mathematical operation used is

$$A = -\log(\%T/100) = \log(X/B).$$

The default value for the y-axis scale is 0 to 2.4. Normally the sample spectra should be taken in this mode [14].

3.4 Baseline Correction of Spectra

We have taken the plots of the complete spectra over the spectral range 4600–400 cm^{-1}. The important features in our spectrum are in the range 1400 – 400 cm^{-1}, so we have taken the expanded plots of the spectra in this region. These spectra were not with the corrected baseline, so we have to correct the baseline of these spectra.

Baseline correction operates on the sample file. Subtractions and baseline corrections should always be done in absorbance mode (display format=3). To do the baseline correction of the spectra, we do the following:

Go to main menu.

We press the main menu item number 4- subtraction/ baseline correction. There are three baseline correction commands available, i.e., level correction, Ramp correction and curve correction. Although the level function occurs first on the menu, the recommended order is Curve, Ramp and then Level. These correction commands are described below.

(i) Curve Correction

For curve correction, we press the menu item number 8. This command corrects the curvature in the baseline, either in entire spectrum or selected portion of the display. Press Y to continue the curve correction. Now press <Alt Cursor> key and Roll (↑, ↓) key simultaneously to adjust the value of FCR (scaling factor for reference file) until the curvature in the baseline is straightened. If necessary, slow the rate of change of FCR by changing DFCR from default value 0.01 to 0.001 or less. To finish the baseline correction press Y.

(ii) Ramp Correction

This command corrects the slope in baseline, either in entire spectrum or the selected portion of the display. Repeat the above procedure again until the spectrum is straightened.

(iii) Level Correction

We press the menu item number 6 for operation of this command. This command changes the baseline level of the entire spectrum. The level function operates on the whole spectrum in the absorbance to change the baseline level with respect to y-axis. We use <Alt Cursor> key and RollKey (↑, ↓) simultaneously to adjust the level of the spectrum. To continue the operation, we press <Space Bar>. To finish with the baseline correction, press Y. Now press 0 to exit to main menu.

3.5 Storage/Retrieval of Data

After the collection of data, we have to store the data. This can be done by using DX-FTIR program. From the main menu, we select menu item number 6- Disk storage/Retrieval. Now mount the floppy disk in a drive and then select 3-Mount floppy # 1. To store the data on a floppy disk, we select item number 1-Store Named File from the Disk Storage/Retrieval menu. A listing of the files of the current directory appears. Select the required data file and enter the filename A valid filename consists of twelve alphanumeric characters. The first character must be alphabetic, and one period (.) may be used in the filename. In our measurements, we have used both alphabetic as well as numeric characters for the filename.

To retrieve the stored data, we select item # 2- Retrieve Named File, from the Disk Storage/Retrieval menu. Now select the required file to which the data is to be retrieved before typing the filename. The filename typed must exactly match the filename listed in the mounted directory, otherwise the data retrieval is not possible.

3.6 Plotting the Data

After the data has been collected, we have to plot the data in a plotter. For this we first go to the main menu and then select item # 3- plot data. From the plot data menu, we first choose option 5- view/change parameters to change the necessary parameters. After changing the parameters, we have to initialize plotter, from the plot data menu. Now we enter the required option, which we want to plot, i.e. plot sample, plot background or plot interferogram. As we select the particular option, the plotter begins to plot the data. The background spectrum is always plotted in emittance versus warenumbers (cm^{-1}), where as sample spectrum can be plotted in emittance, % transmittance or absorbance versus wavenumbers (cm^{-1}) [14].

In our spectra, we have plotted all the spectra in absorbance versus wavenumbers. Wavenumbers are along x-axis where as absorbance is along y-axis.

CHAPTER 4

RESULTS AND DISCUSSION

4.1 Introduction

The FTIR absorption spectroscopy provides information on the vibrational modes. Each absorption peak corresponding to a particular frequency in the spectrum represents a particular defect in the sample. That is why, the IR absorption spectroscopy is found to be a sensitive probe for the characterization of defects in semiconductors.

We studied different samples of silicon (Si) which were grown by Czochralski (CZ) as well as float-zone (FZ) techniques. As discussed earlier in Chapter 3, during the growth process, some impurities are introduced unintentionally in silicon. In CZ-grown samples the major impurities incorporated are oxygen and carbon. In float-zone samples the oxygen concentration is greatly reduced but carbon is still present.

We obtained the infrared absorption spectra of various silicon samples. All the spectra were taken at room temperature using a Nicolet Fourier transform infrared (FTIR) spectrometer 20-DXB, equipped with TGS (triglycerine sulphide) detector and a germanium coated KBr beam splitter. The spectra were taken in the wavenumber range 4600-400 cm^{-1} with the spectral resolution of 1 cm^{-1}. The spectra were generally obtained by averaging over 500 scans, whereas the background spectra were obtained by averaging over 300 scans. The background spectrum was taken with out any sample in the sample comportment after careful flushing of the spectrometer with dry

compressed air. The sample spectrum was ratioed to the background spectrum and, in absorbance mode, can be computed as follows:

Absorbance $A = -\log(X/B)$

Where

'X' is the single beam spectrum of the sample

'B' is the background spectrum.

The spectra were stored and then the desired portions of the spectra were displayed and plotted. The baseline correction of the sample was done using curve, ramp and level corrections, respectively. The spectral features of interest in Si are known to lie in the spectral range 1400-400 cm^{-1}. No important feature was observed beyond this range. So we concentrated on the absorption spectra in this range for our work.

4.2 Results and Analysis

4.2.1 A: Float-Zone Silicon

1. p-type Silicon (p Si 106 FZ sample)

The FTIR absorption spectrum for this sample, taken in the wavenumber region from 4600 to 400 cm^{-1} is shown in Fig. 4.1. The spectrum displays a strong peak in the vicinity of 600 cm^{-1}. The detailed features of this spectrum were explored by expanding the spectrum in the spectral range from 1400–400 cm^{-1}. The "Baseline Correction" was performed by employing the "Curve", "Ramp"and "Level" correction commands. The expanded and corrected spectrum is shown in Fig. 4.2. This figure shows a prominent peak at around 610 cm^{-1} with shoulders on either side around 620 cm^{-1} and 605 cm^{-1}. In this spectrum about five smaller peaks are also

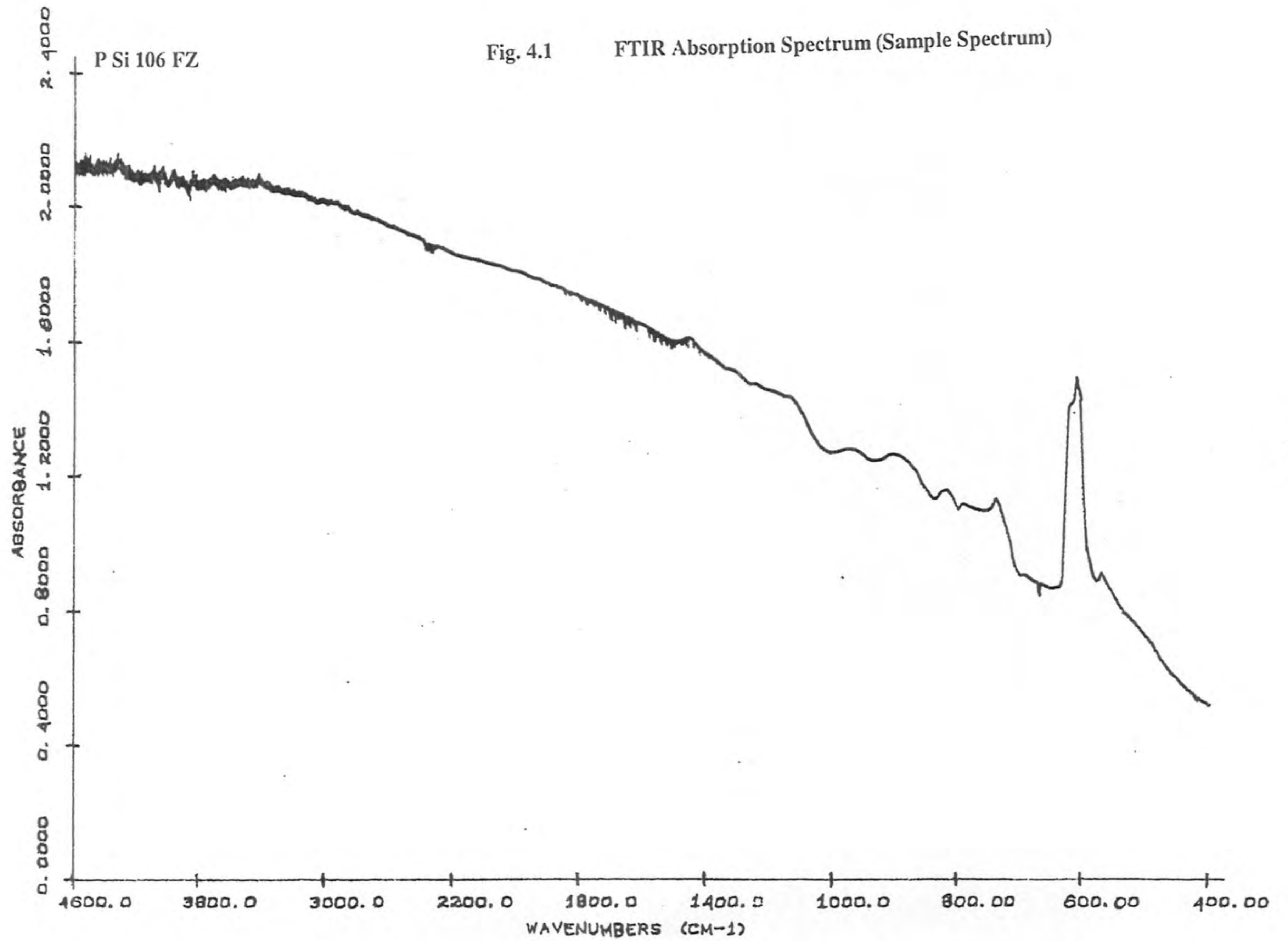

Fig. 4.1 FTIR Absorption Spectrum (Sample Spectrum)

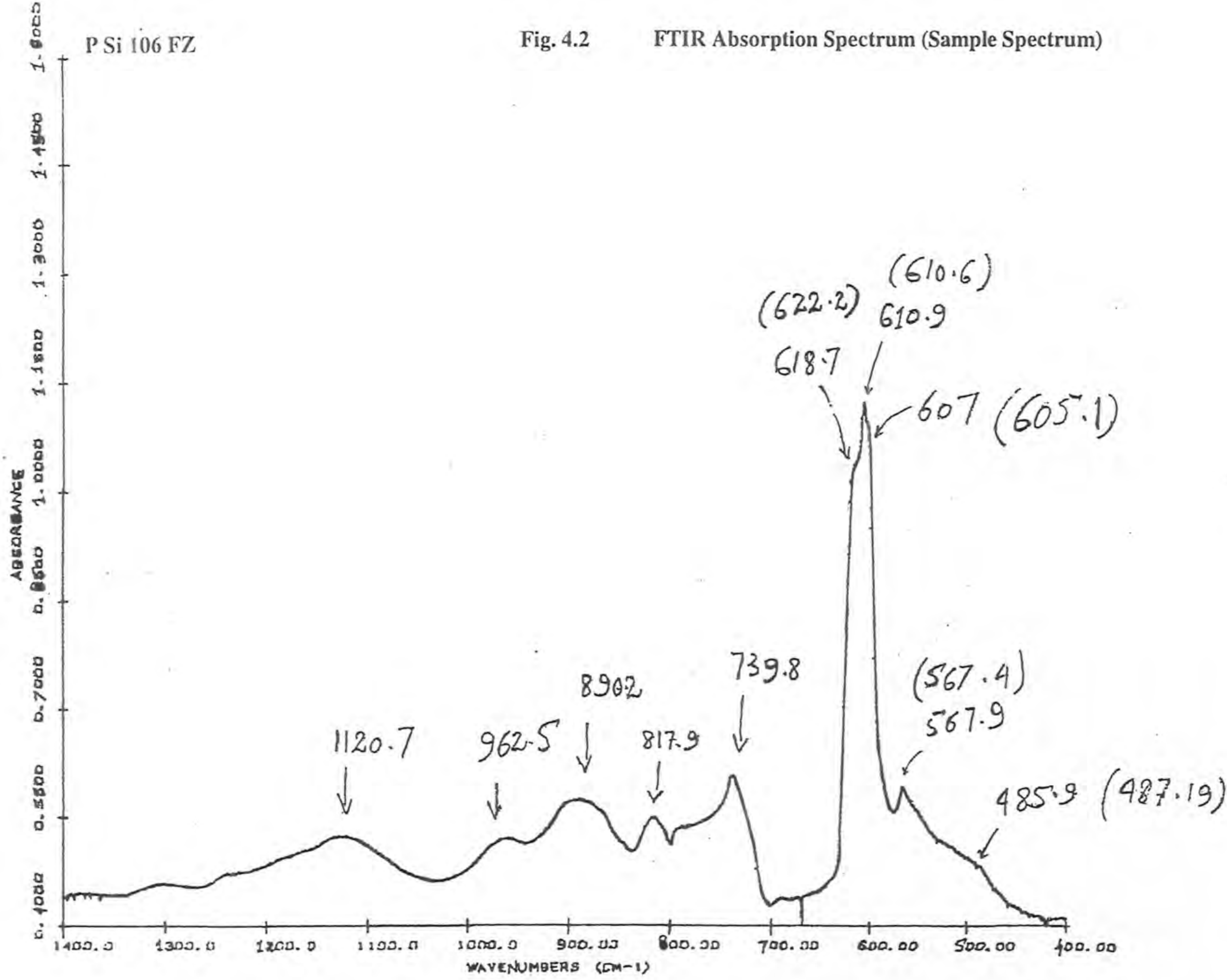

Fig. 4.2 FTIR Absorption Spectrum (Sample Spectrum)

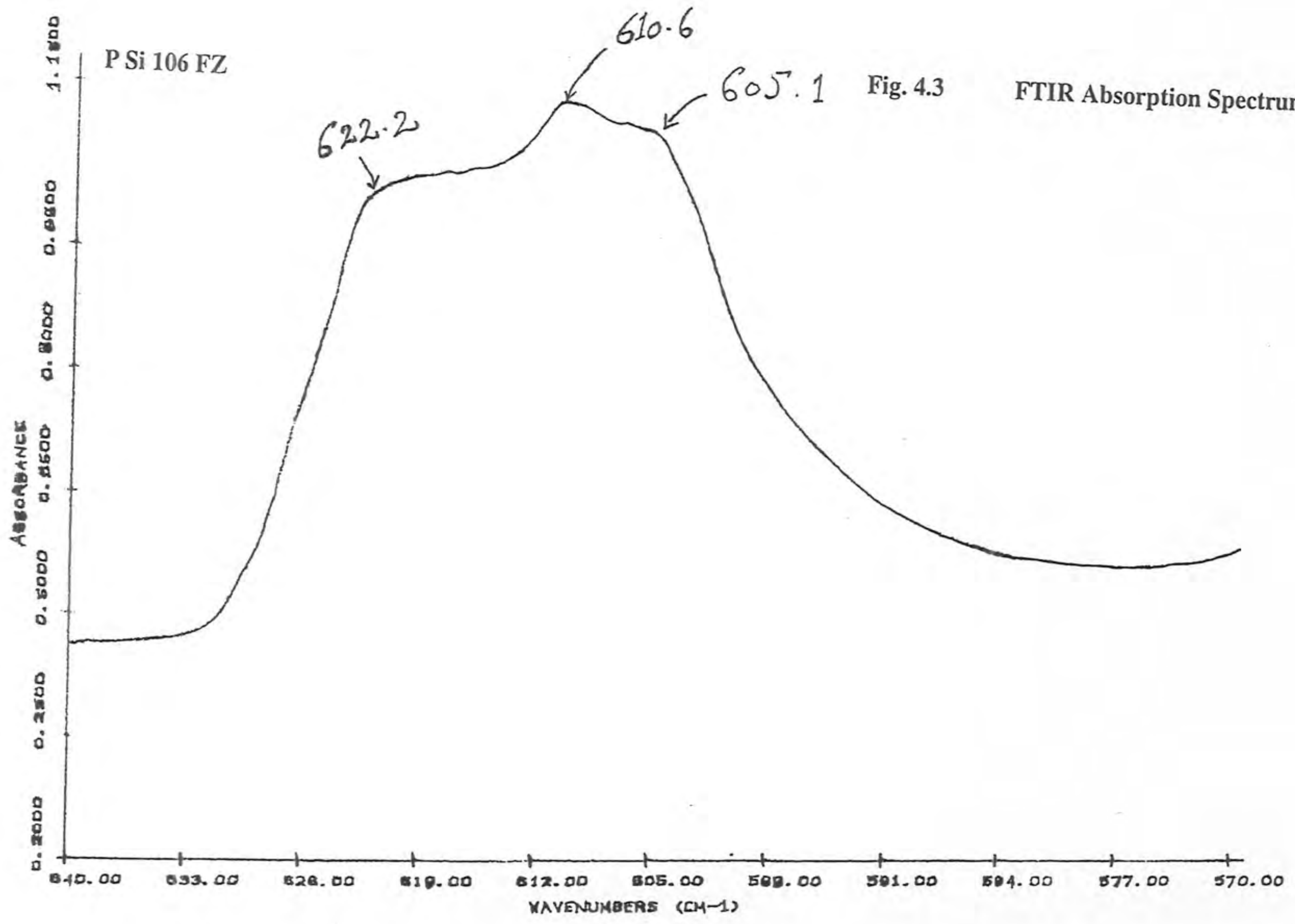

Fig. 4.3 FTIR Absorption Spectrum (Sample Spectrum)

observed at wavenumbers 567.4, 739.8, 817.9, 890.2, 962.5, and 1120.7 cm^{-1} respectively.

The feature at 610 cm^{-1} was further explored by expanding the spectrum in the range 640–570 cm^{-1}. The shoulders have been resolved and are shown in Fig. 4.3. This figure clearly shows two broad humps at 605.1 cm^{-1} and 622.2 cm^{-1}.

2. n-type Silicon

We have also studied the FTIR absorption spectra of three n-type silicon samples. The absorption spectra of these samples, taken in the wavenumber region from 4600 to 400 cm^{-1} are shown in Figs. 4.4, 4.5 and 4.6. All the three spectra display strong peaks in the vicinity of 600 cm^{-1}. The detailed features of these spectra were again explored by expanding in the spectral range from 1600-400 cm^{-1}. The Baseline correction of these spectra was performed by employing Curve, Ramp and Level Correction Commands. The expanded and corrected spectra are shown in the figures 4.7, 4.8 and 4.9. The prominent features of these spectra are almost similar for the three n-type samples. A sharp absorption peak at 610 cm^{-1} with shoulder at 621.5 cm^{-1}, is present in these spectra. We again observe smaller peaks at 566.4 cm^{-1}, 739.8 cm^{-1}, 817.8 cm^{-1}, 889.8 cm^{-1}, 962.5 cm^{-1}, 1121.9 cm^{-1}, 1233.6 cm^{-1}, 1302.3 cm^{-1} and 1450 cm^{-1}. However, a noticeable difference in Fig. 4.8 was observed, which is the presence of a small and broad peak about 1233.6 cm^{-1} that is not present in samples of Fig. 4.7 and Fig. 4.9. We will discuss this point in section 4.3.

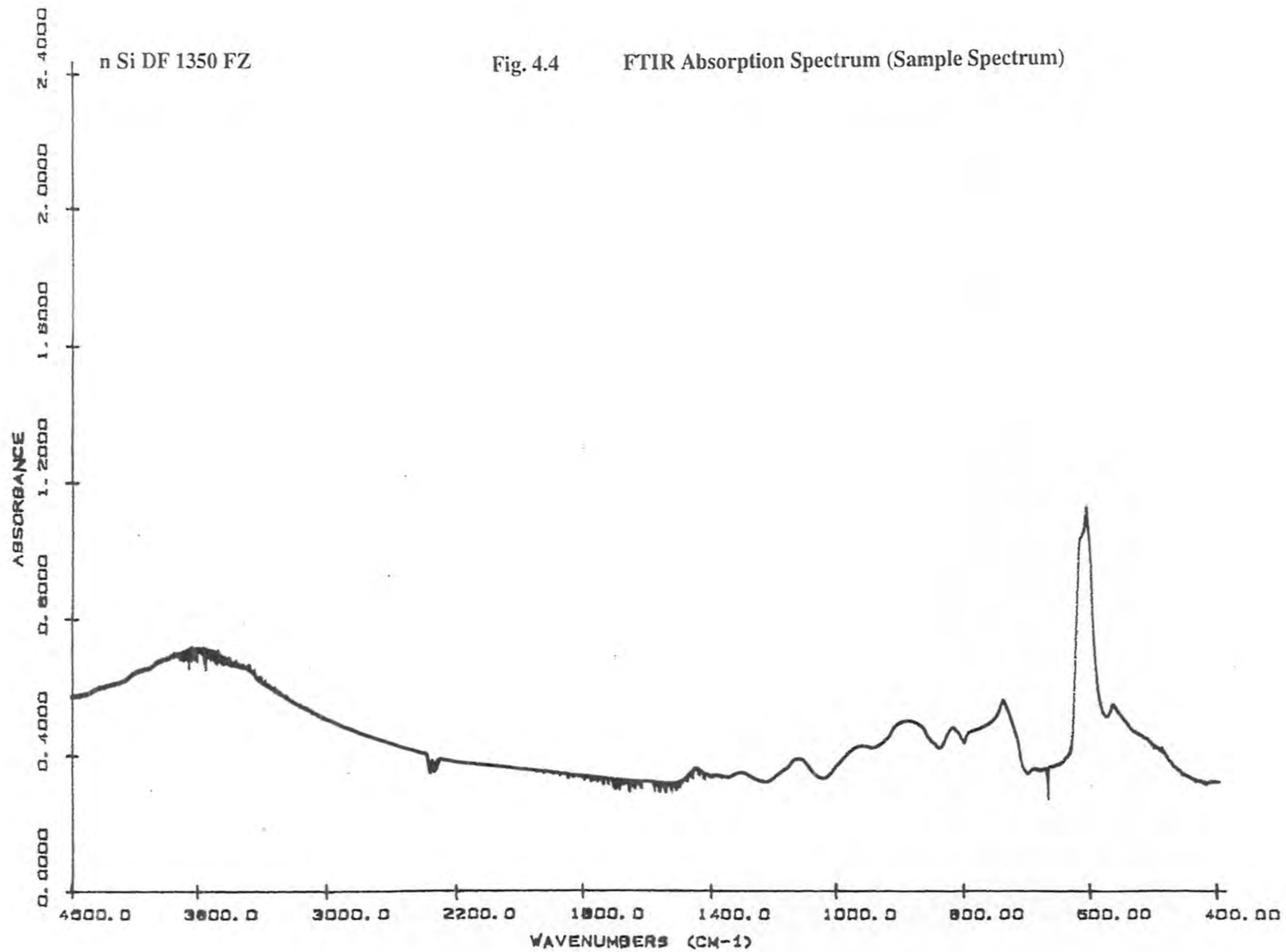

Fig. 4.4 FTIR Absorption Spectrum (Sample Spectrum)

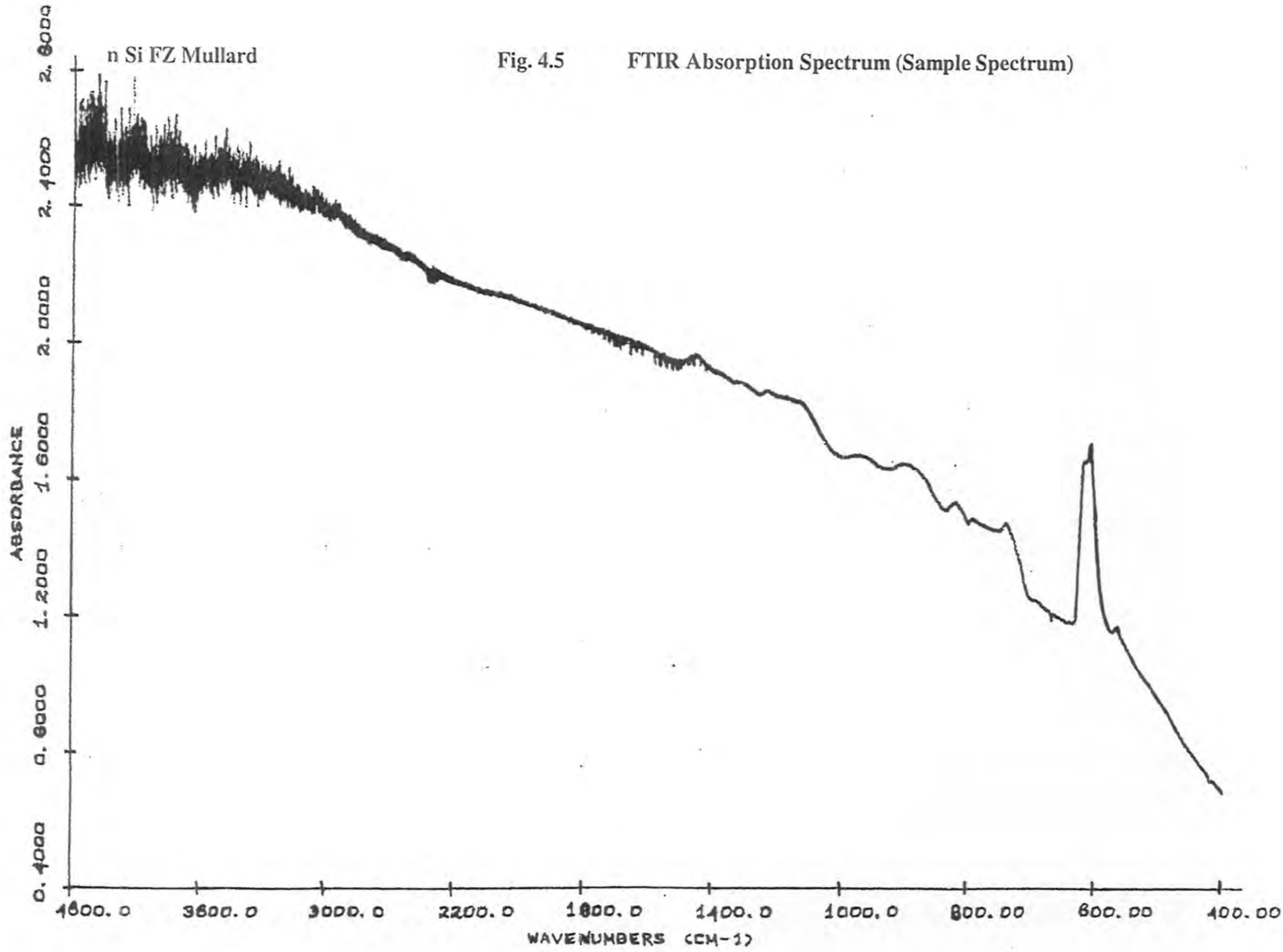

Fig. 4.5 FTIR Absorption Spectrum (Sample Spectrum)

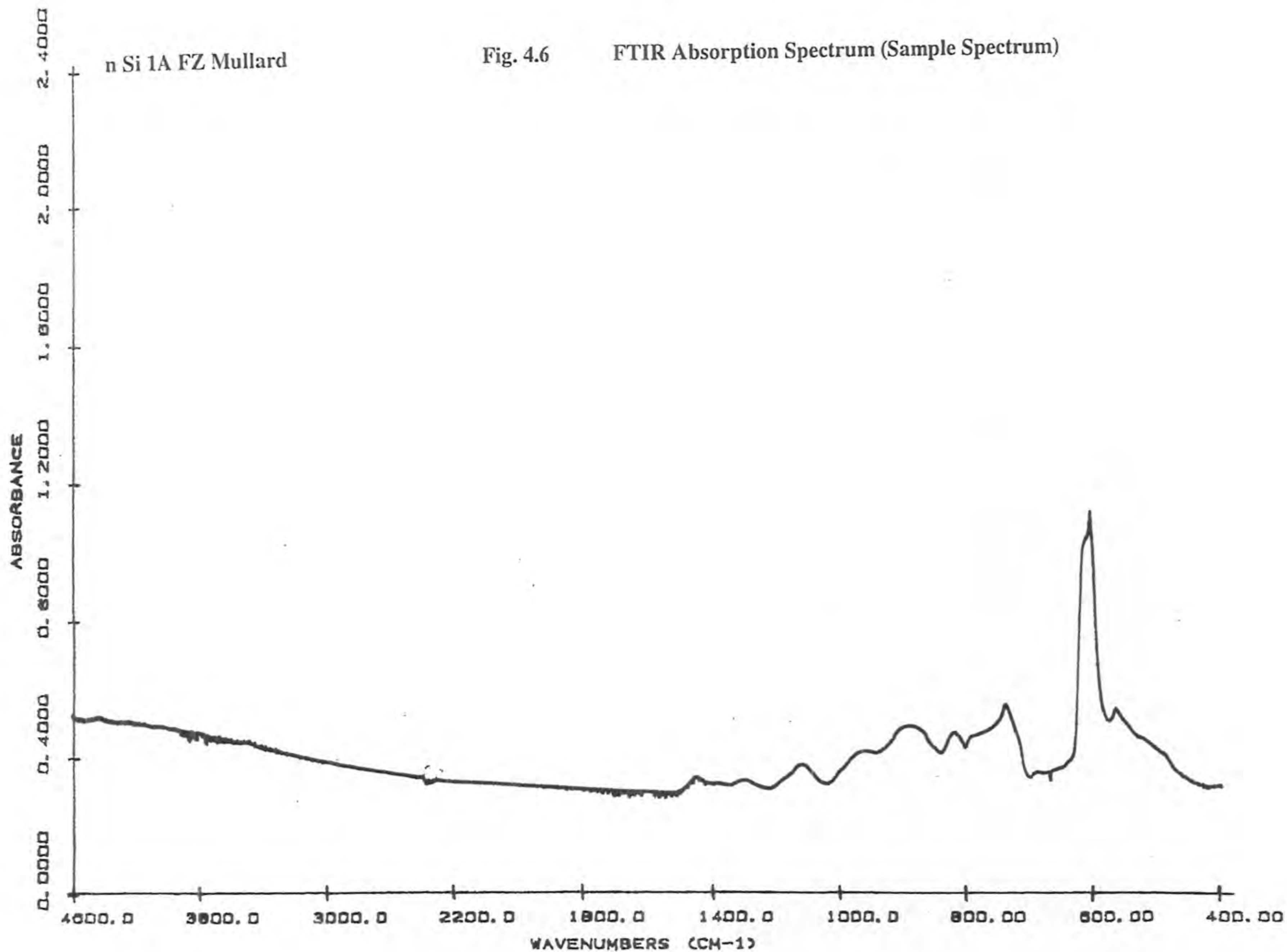

Fig. 4.6 FTIR Absorption Spectrum (Sample Spectrum)

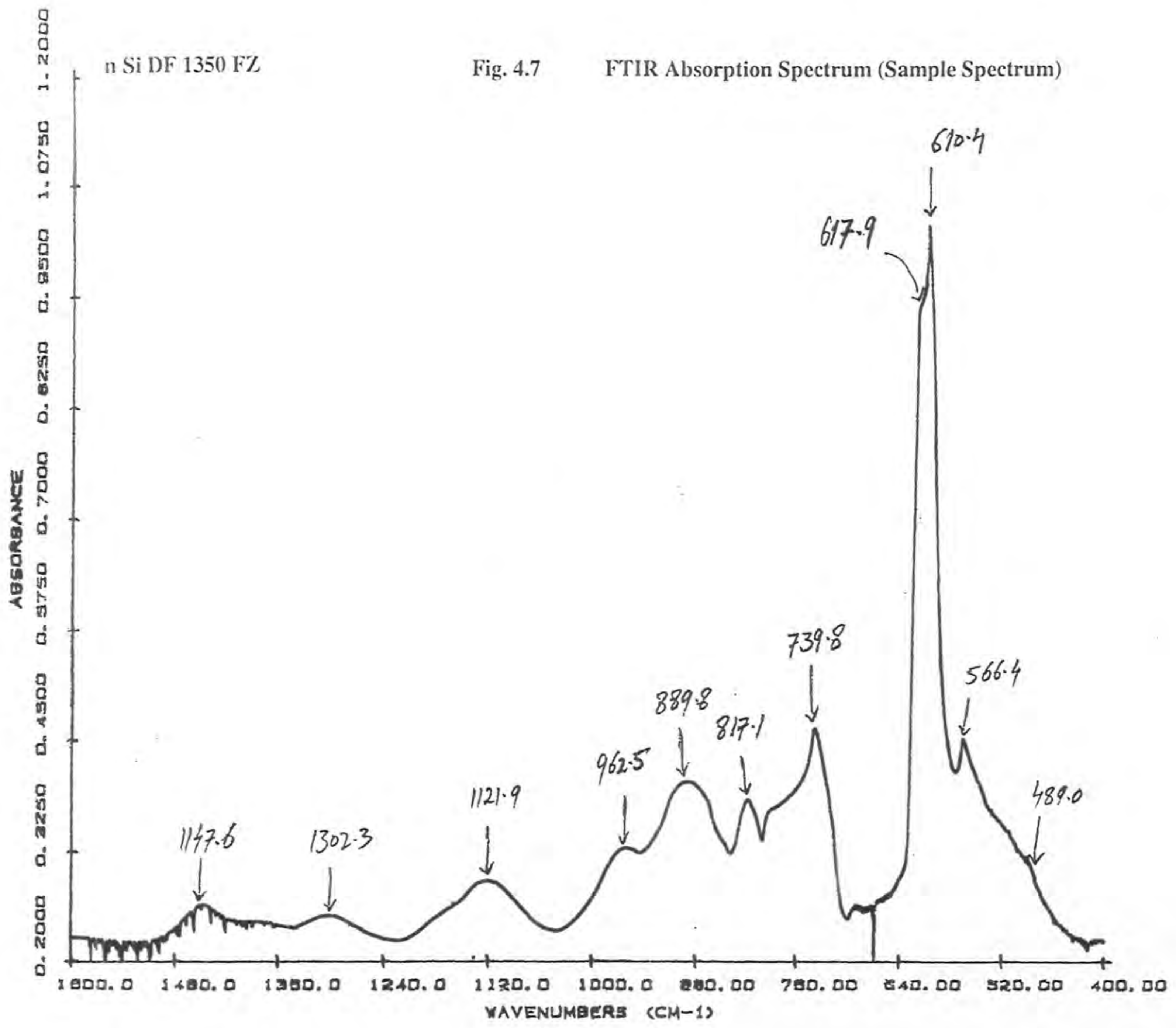

Fig. 4.7 FTIR Absorption Spectrum (Sample Spectrum)

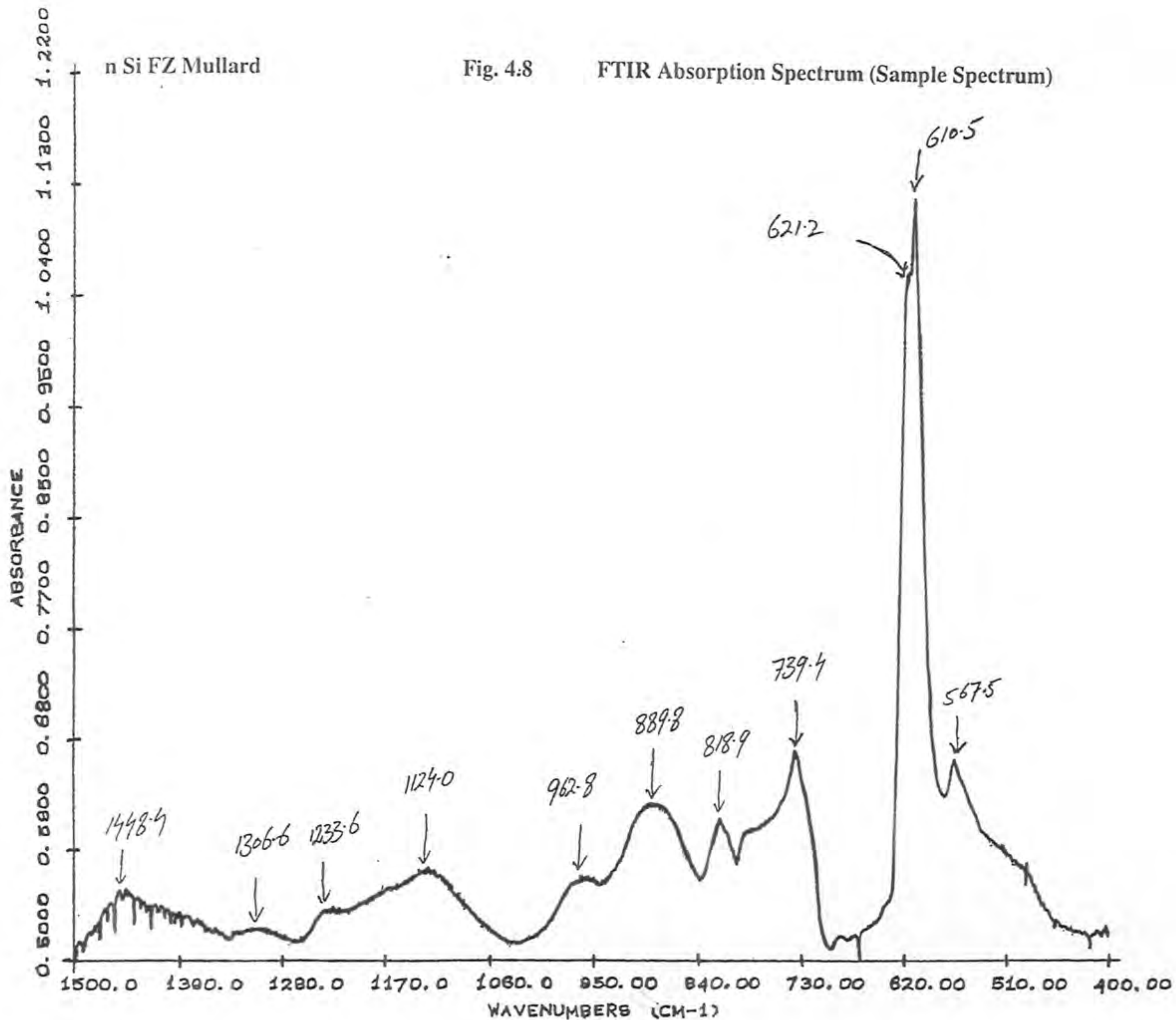

Fig. 4.8 FTIR Absorption Spectrum (Sample Spectrum)

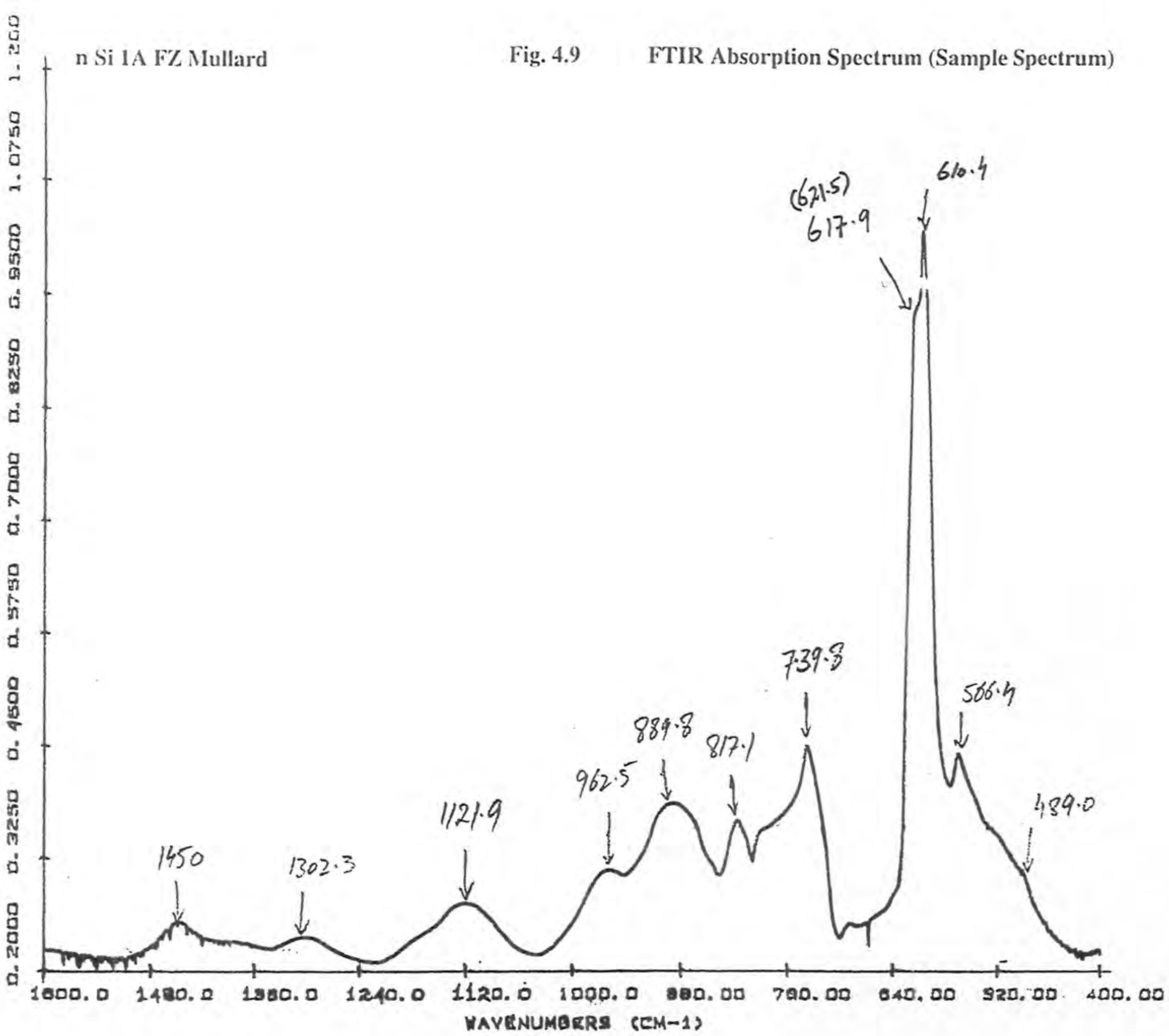

n Si 1A FZ Mullard

Fig. 4.9 FTIR Absorption Spectrum (Sample Spectrum)

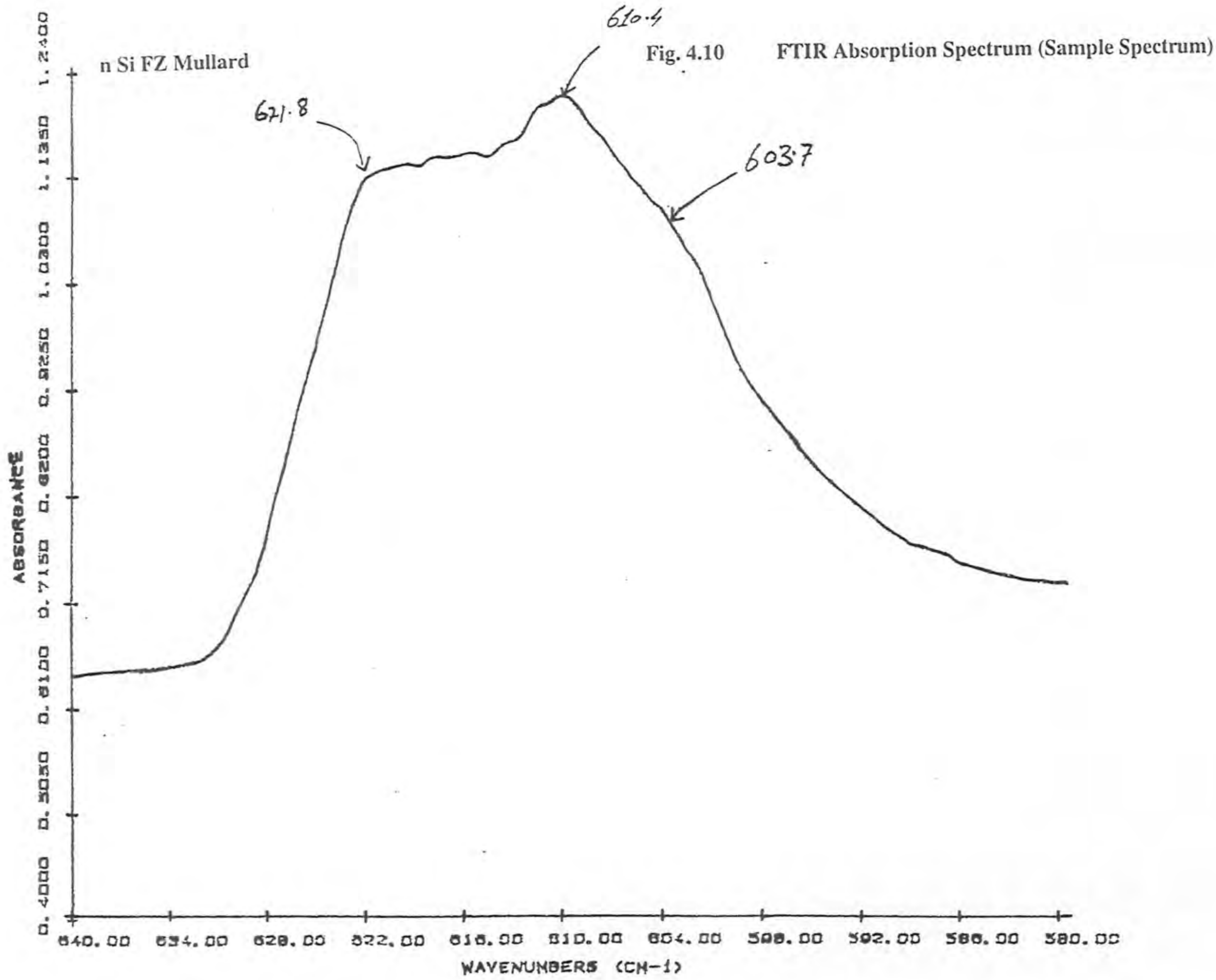

Fig. 4.10 FTIR Absorption Spectrum (Sample Spectrum)

3. Si High Carbon Low Oxygen (Si HCLO sample)

The spectrum of this sample is show in Fig. 4.11. A very interesting feature was observed in this spectrum. The prominent peak which is present at around 610 cm^{-1} in all other FTIR spectra shown earlier, has been shifted and now appears at 605.7 cm^{-1}. In the expanded spectrum, Fig. 4.12, a very sharp peak at 605.7 cm^{-1} with shoulders at 610.9 cm^{-1} and 622.5 cm^{-1} is also observed. The other smaller features were observed at around 567.5 cm^{-1}, 739.4 cm^{-1}, 818.9 cm^{-1}, 884.8 cm^{-1}, 962.8 cm^{-1}, 1126.2 cm^{-1}, 1304.5 cm^{-1} and 1448.4 cm^{-1}. The peak at 605.7 cm^{-1} was again investigated by further expanding the spectrum in the wavenumber range 635 cm^{-1} to 575 cm^{-1}. This spectrum is shown in the Fig. 4.13.

4. (i) Si-Reference Ultra High Purity Oil Quenched Sample

The spectrum of this sample is shown in Fig. 4.14. The expanded spectrum is shown in Fig. 4.15. The prominent features are similar to those observed earlier in our other samples. The smaller features are the same as in the previous spectra, except the feature at 1087.5 cm^{-1}, which only appears in this oil quenched sample.

(ii) Si-Ag UHP Oil Quenched Sample

The spectrum of this sample is quite similar to the one for the above sample. All the features are similar. The full range spectrum and the expanded spectrum are shown in Figs. 4.16 and 4.18 respectively.

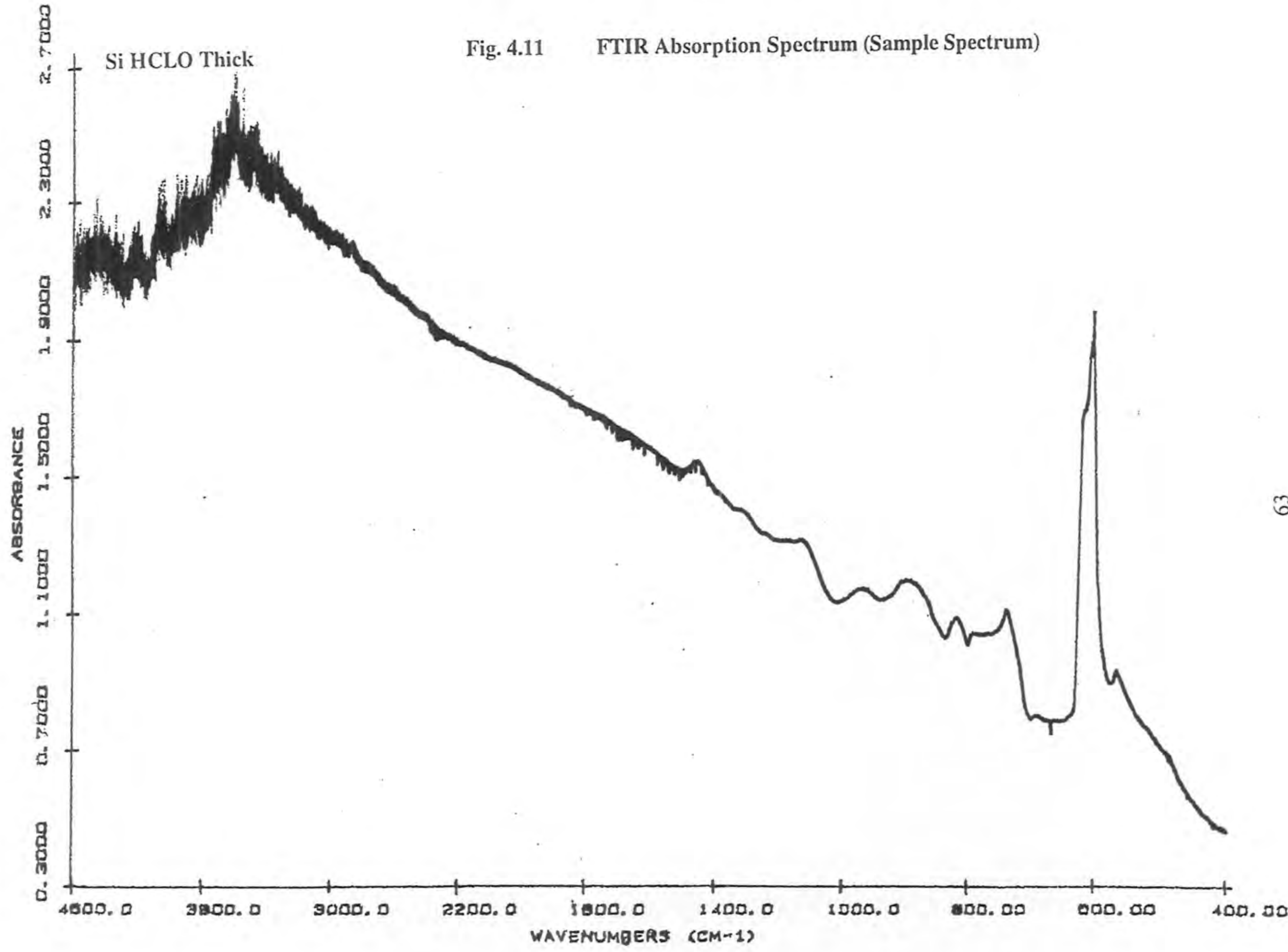

Fig. 4.11 FTIR Absorption Spectrum (Sample Spectrum)

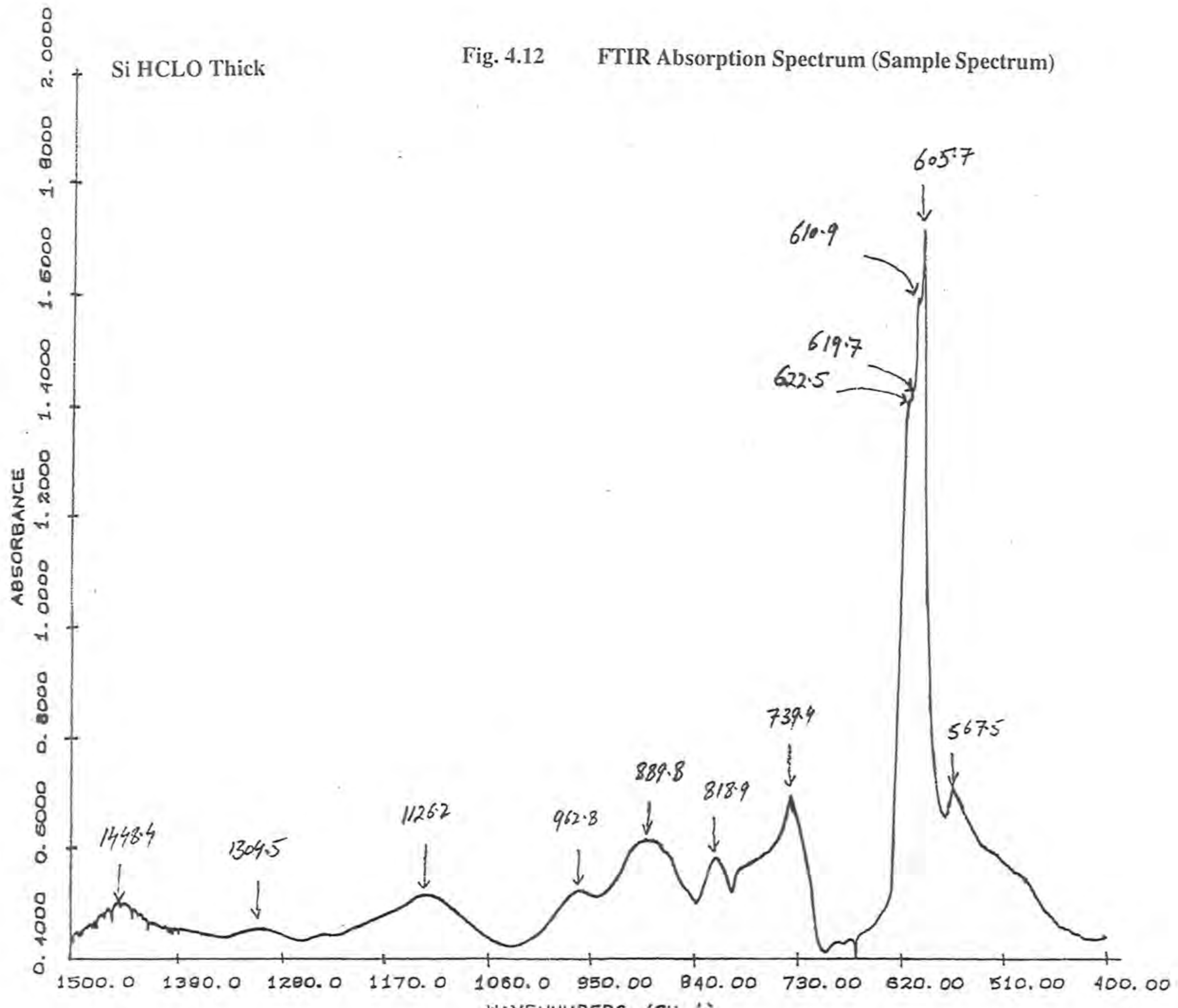

Fig. 4.12 FTIR Absorption Spectrum (Sample Spectrum)

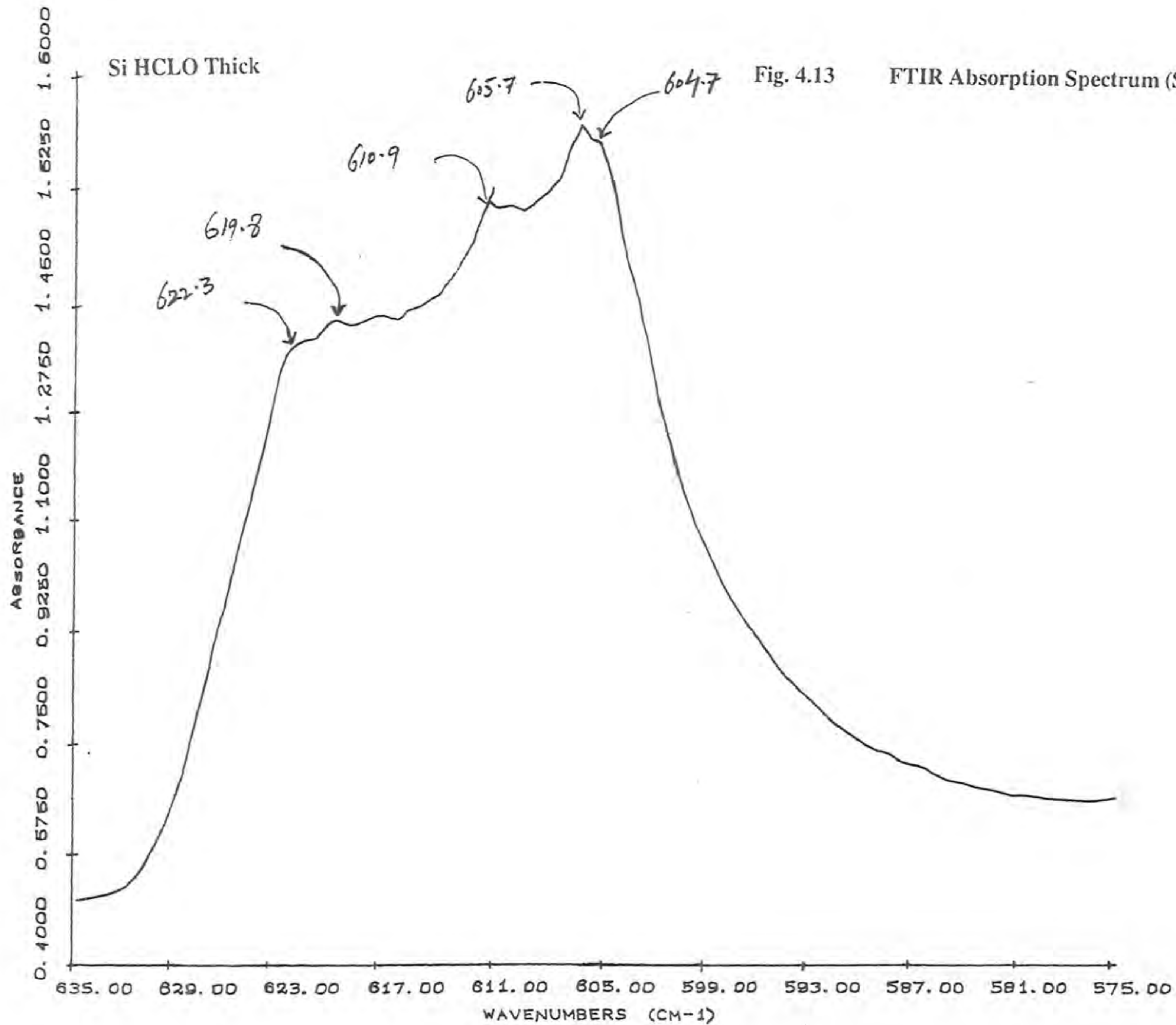

Fig. 4.13 FTIR Absorption Spectrum (Sample Spectrum)

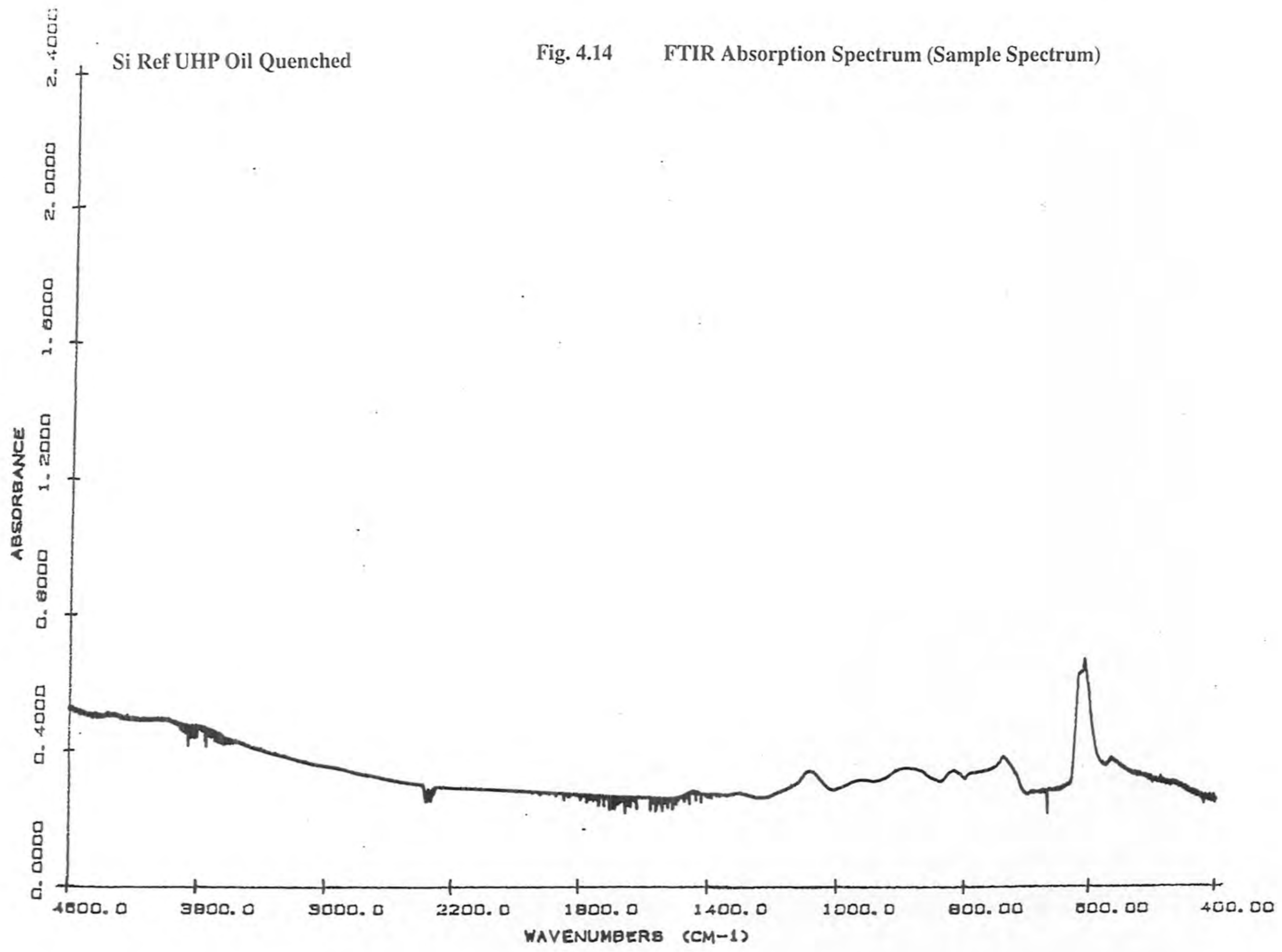

Fig. 4.14 FTIR Absorption Spectrum (Sample Spectrum)

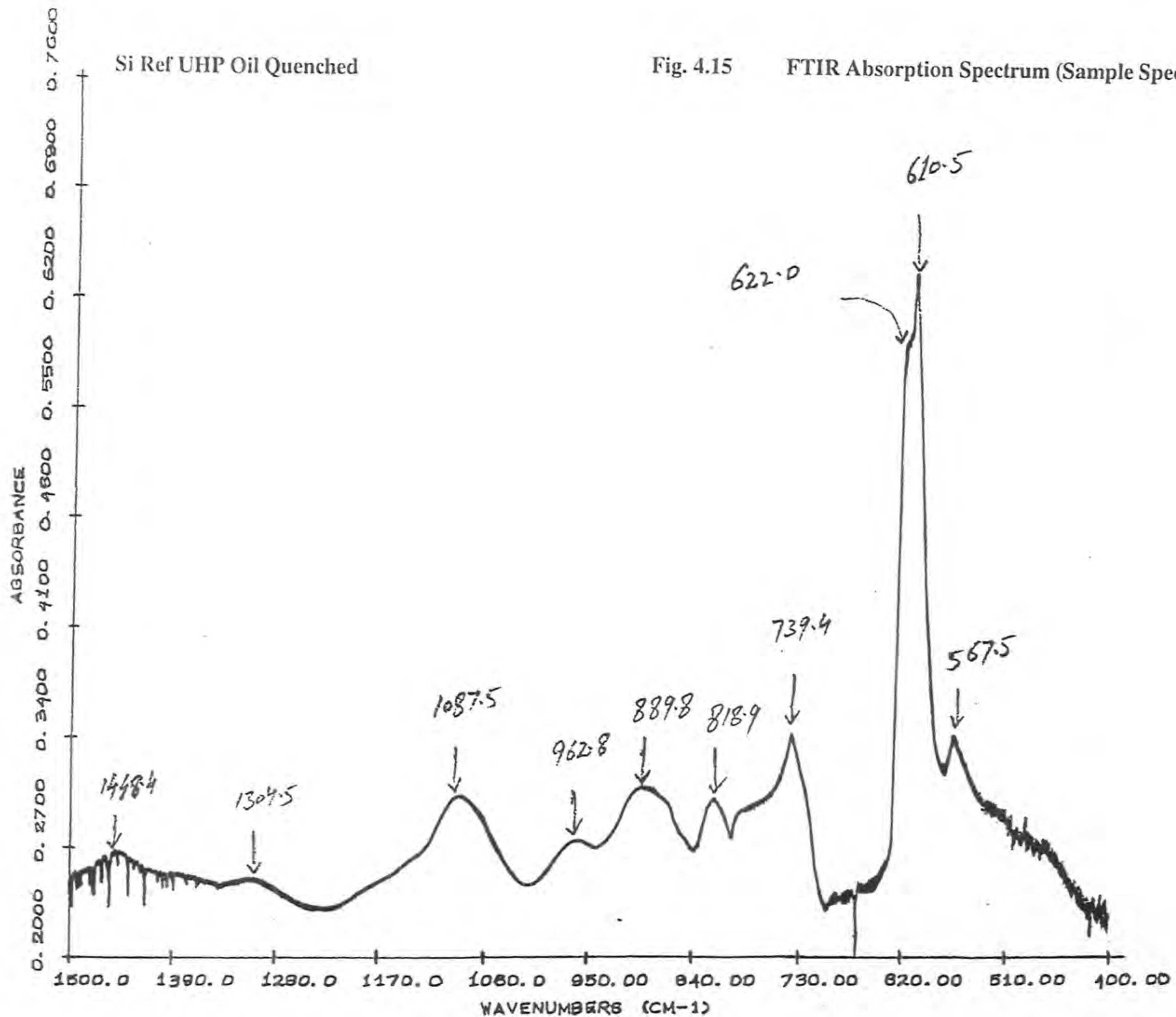

Fig. 4.15 FTIR Absorption Spectrum (Sample Spectrum)

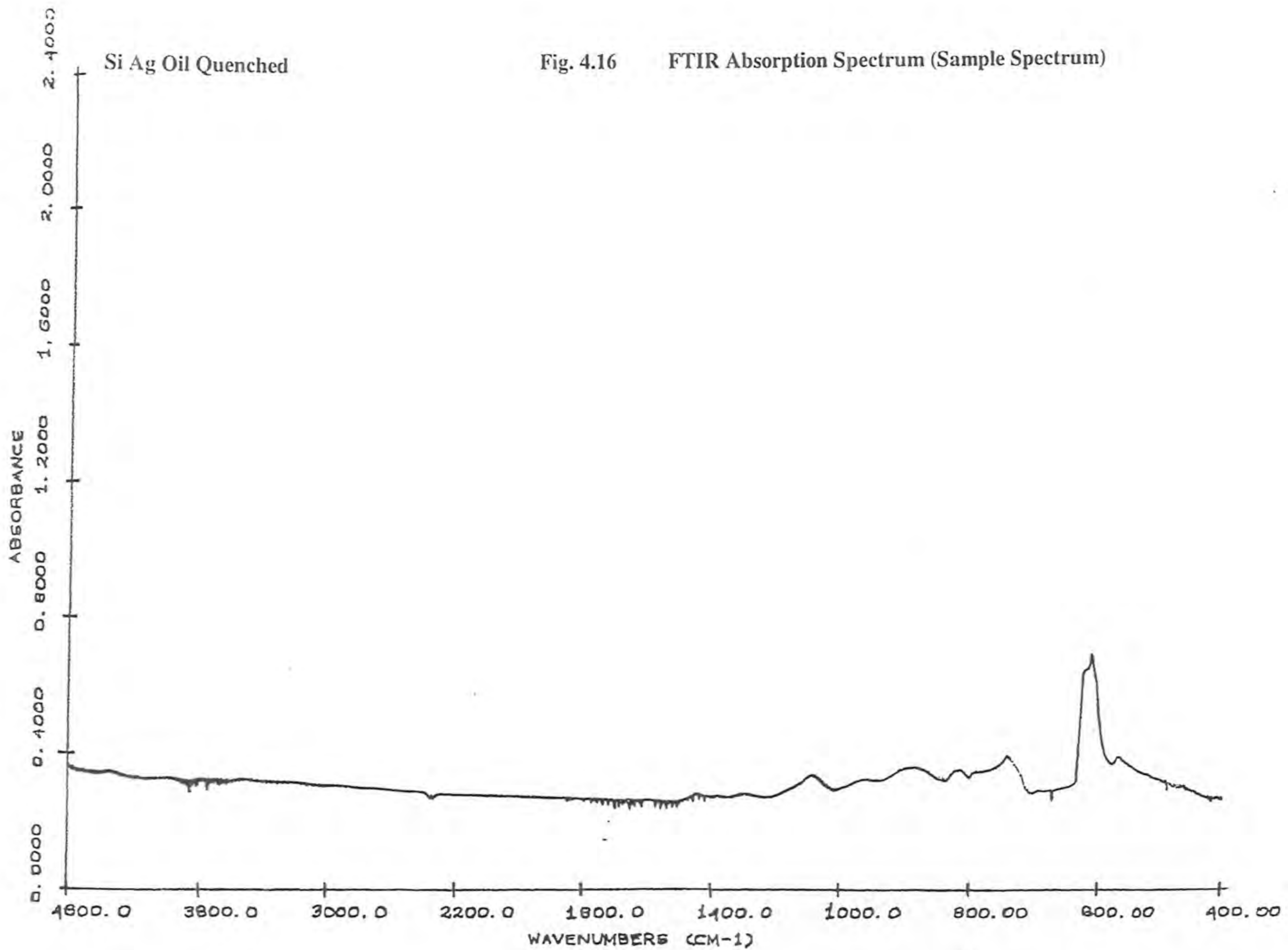

Fig. 4.16 FTIR Absorption Spectrum (Sample Spectrum)

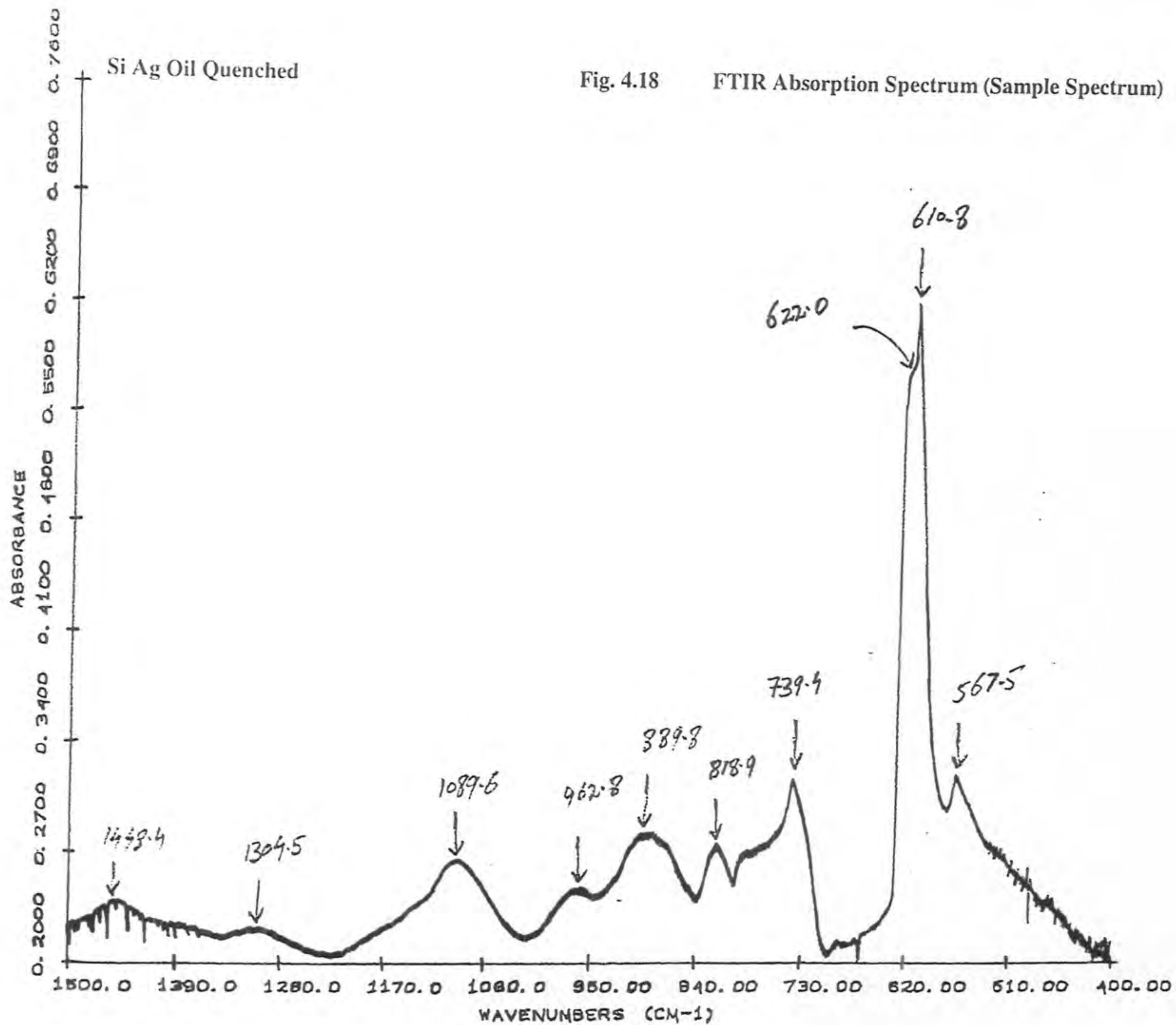

Fig. 4.18 FTIR Absorption Spectrum (Sample Spectrum)

5. Si 30994/64 FZ Sample

The whole spectrum of this sample in the wavenumber region 4600-400 cm^{-1} is shown in Fig. 4.19. The most prominent peak in this spectrum was observed around 600 cm^{-1}. The prominent features were explored by expanding the spectrum in the range of 1600-400 cm^{-1}. This spectrum is shown in Fig. 4.20. In this spectrum a large peak is present at 610.4 cm^{-1} . A shoulder is seen at about 622.2 cm^{-1}. The smaller peaks are present at 566.4 , 739.8, 817.1, 889.8, 962.5, 1121.9, 1302.3 and 1445.3 cm^{-1}.

4.2.2 B: Czochralski (CZ) Silicon Sample (Silicon 522 Big)

The FTIR absorption spectrum of this silicon sample, taken in the wavenmber region 4600-400 cm^{-1}, is shown in Fig.4.21. In this spectrum, two prominent absorption peaks in the vicinity of 600 cm^{-1} and 1100 cm^{-1} were observed. The expanded spectrum of this sample in the range 1400-400 cm^{-1} is shown in Fig. 4.22. In this spectrum, there is a strong peak at 1107.0 cm^{-1} and another peak at 610.9 cm^{-1} with a shoulder at 621.9 cm^{-1}. This shoulder has been resolved by further expanding the spectrum in the range 640-570 cm^{-1}. Fig. 4.23 clearly shows two humps on either side of 610.7 cm^{-1} peak. The other smaller features were present at 513.2 cm^{-1}, 567.9 cm^{-1}, 817.9 cm^{-1}, 890.2 cm^{-1}, 962.5 cm^{-1} and 1234 cm^{-1}.

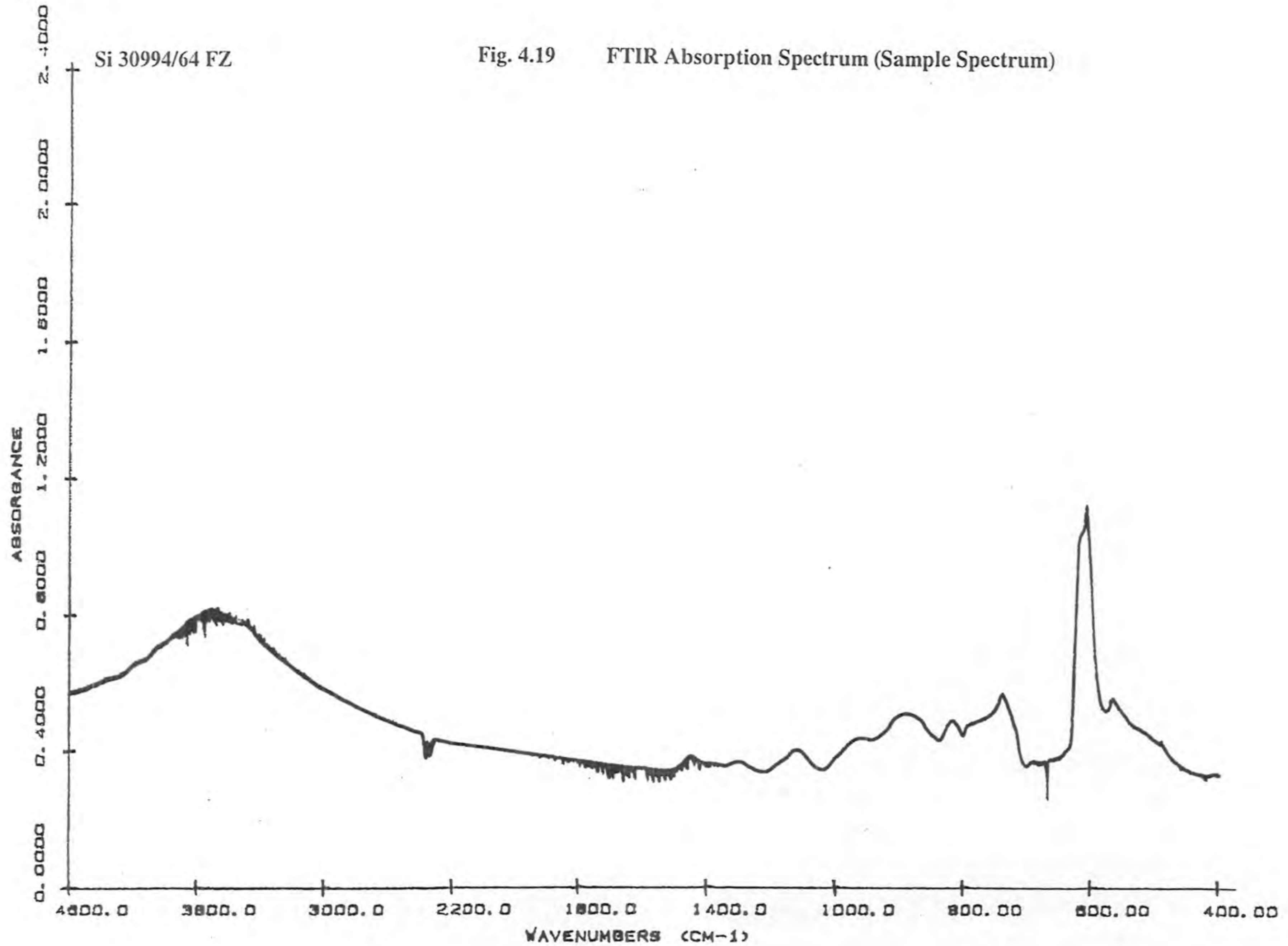

Fig. 4.19 FTIR Absorption Spectrum (Sample Spectrum)

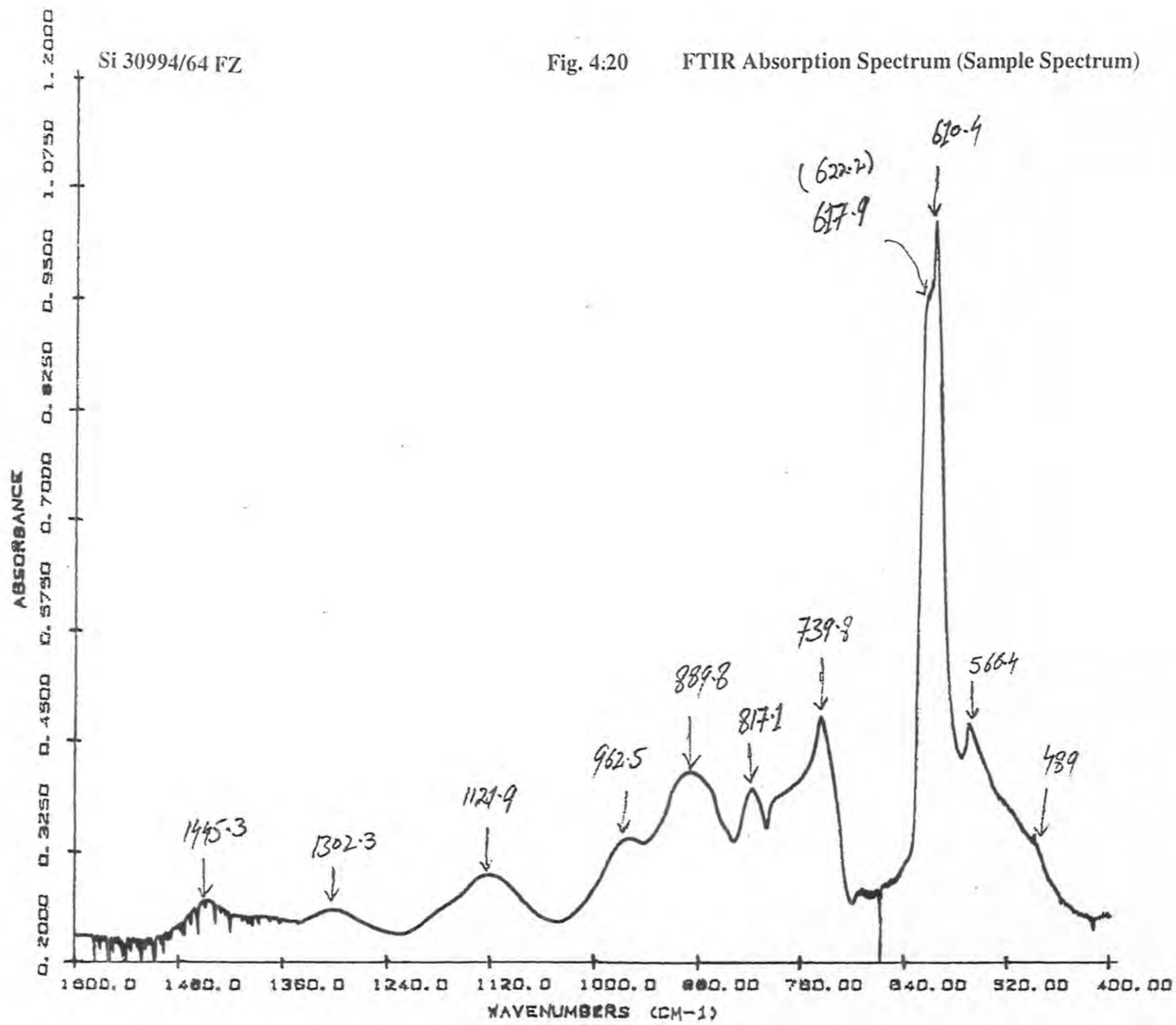

Fig. 4:20 FTIR Absorption Spectrum (Sample Spectrum)

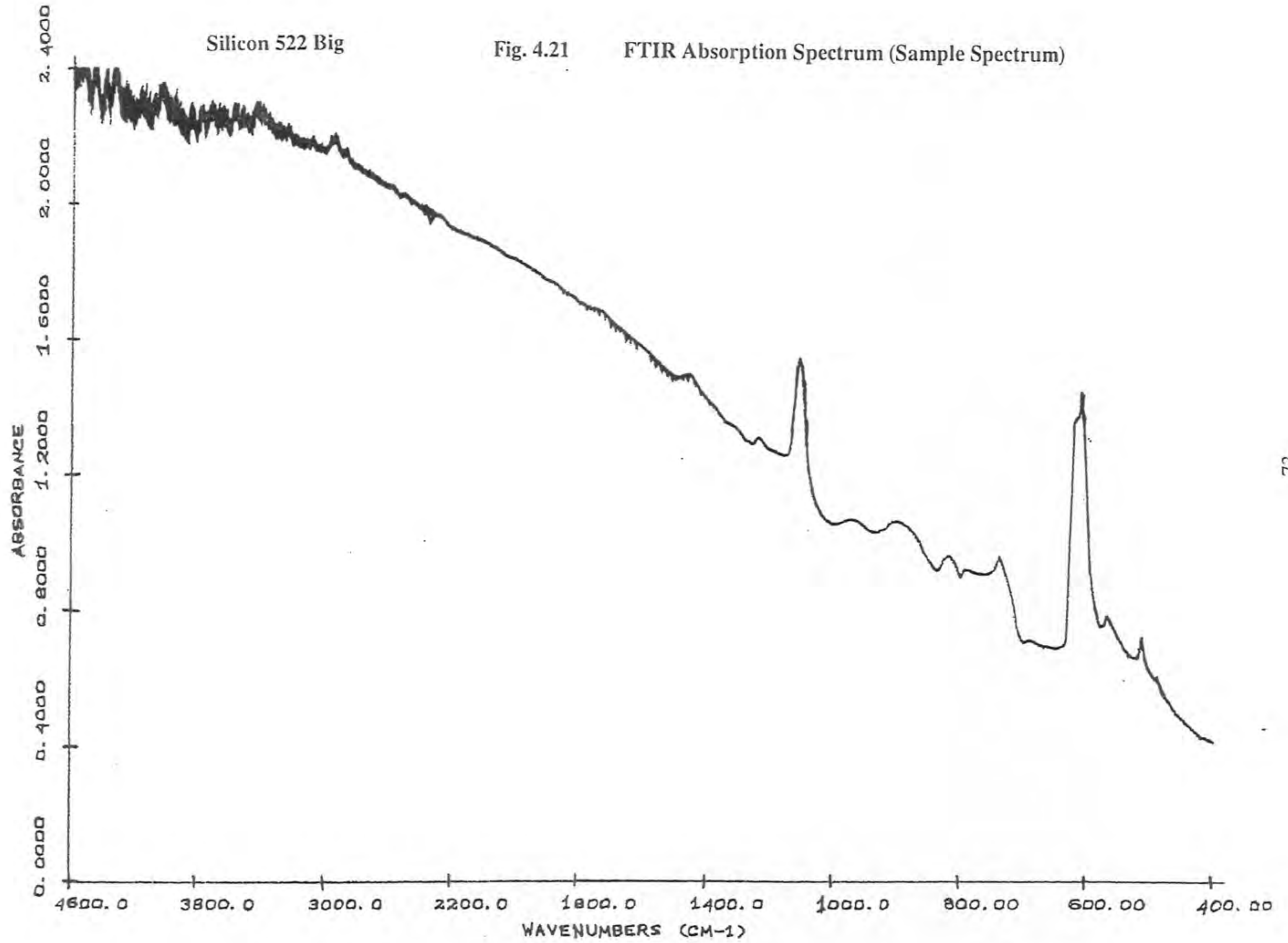

Fig. 4.21 FTIR Absorption Spectrum (Sample Spectrum)

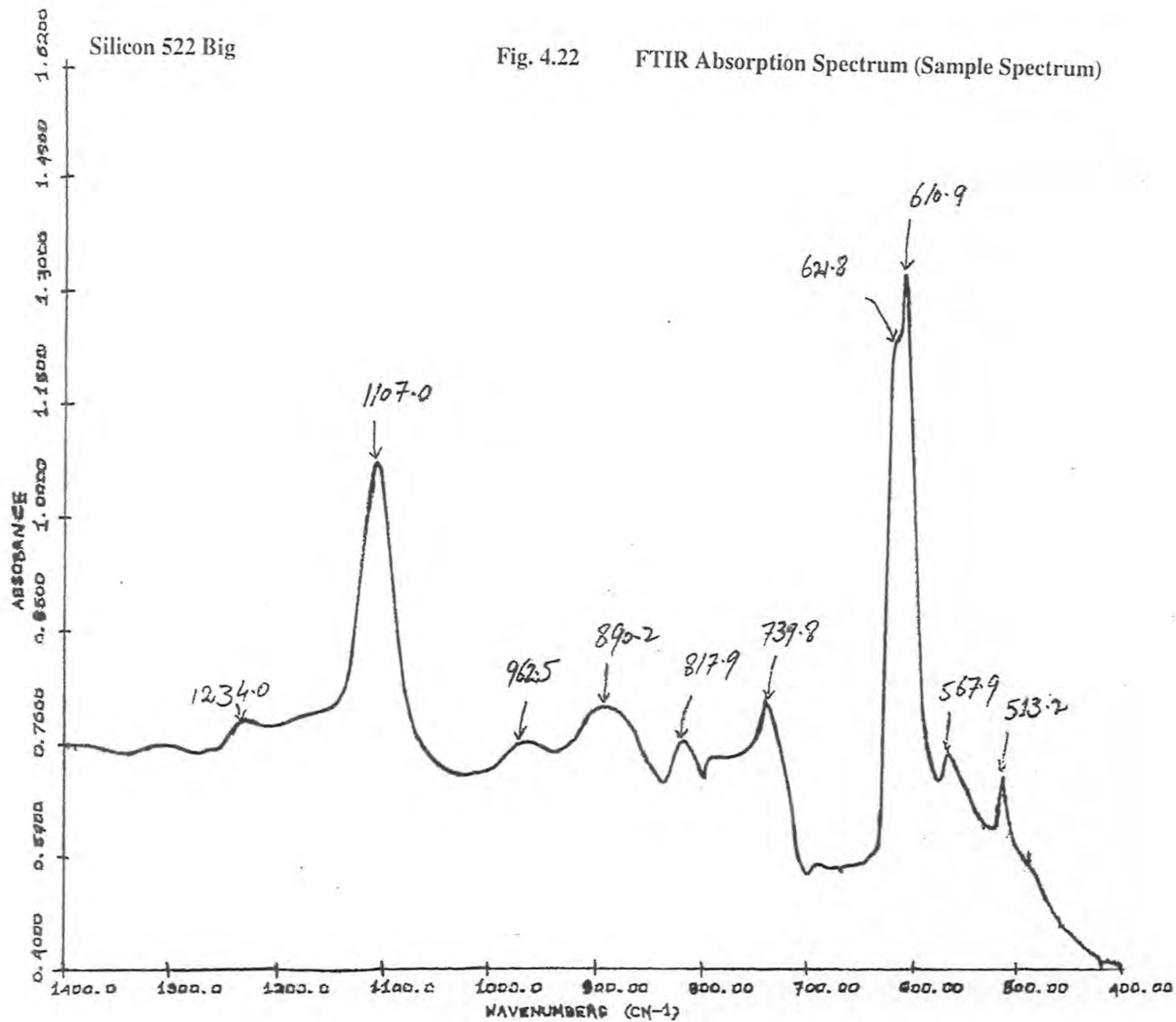

Fig. 4.22 FTIR Absorption Spectrum (Sample Spectrum)

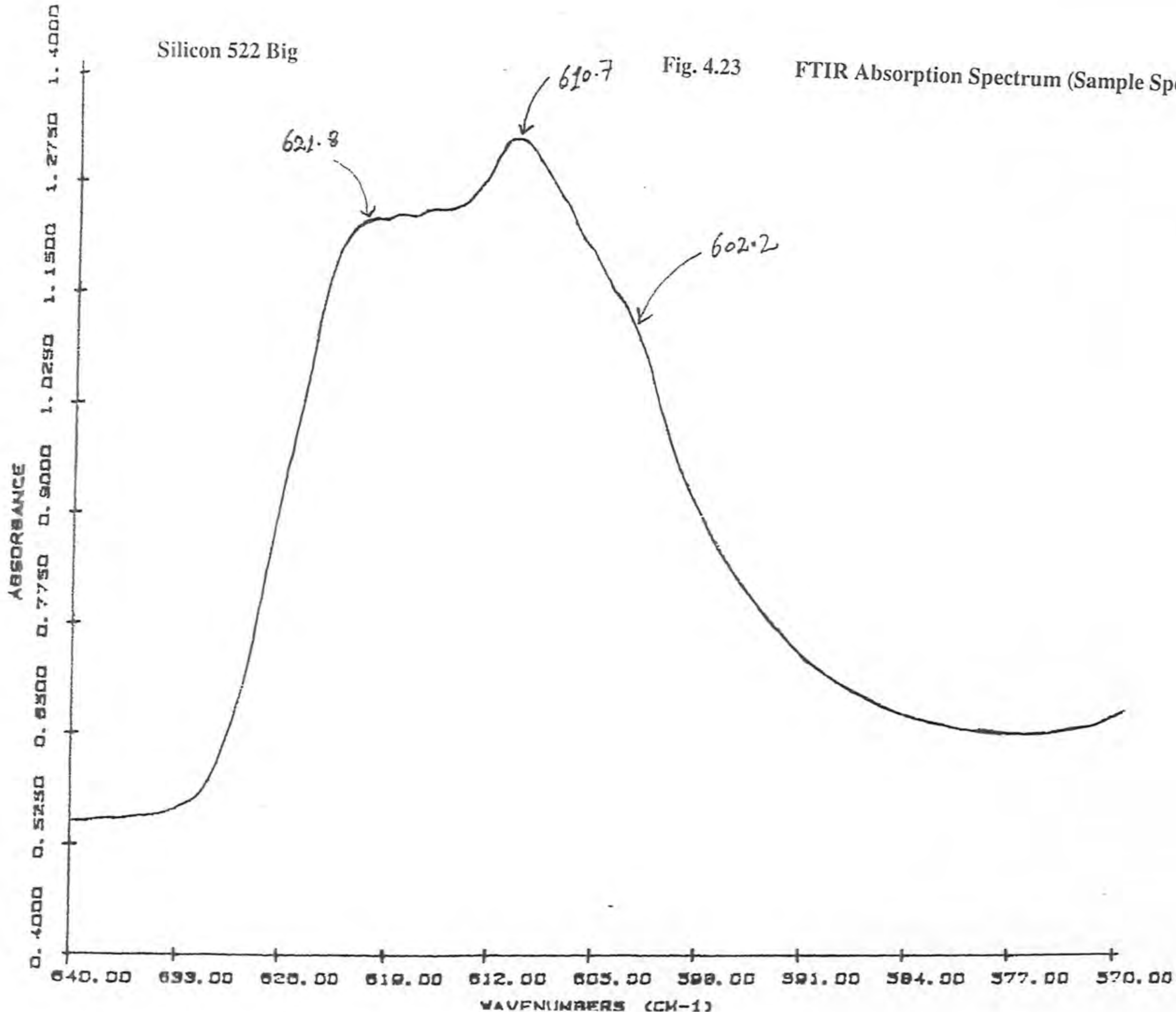

Fig. 4.23 FTIR Absorption Spectrum (Sample Spectrum)

4.3 Discussion

4.3.1 Effects of Oxygen Concentration on Vibrational Modes

We have investigated two sets of silicon samples, CZ-grown silicon samples and Float-zone (FZ) silicon samples, by performing FTIR spectroscopy in the absorption mode. It is well known that oxygen is a common inadvertent impurity in silicon. Most of the O atoms occupy bonded interstitial sites (Oi), binding two host lattice atoms (Si-O-Si) [15]. However, it has been suggested [16] that O could also occupy substitutional site in the silicon lattice. Additionally it has been postulated [17] that gas-like oxygen molecules (O_2) without bonds to silicon atoms exist in dynamical equilibrium with O_i and also that unbonded [18] interstitial oxygen atoms exist as a metastable state of the ground state which is the usual Si-O-Si bridge. Oxygen molecules and single oxygen atoms are supposed to have a much higher migration ability than bound interstitial atoms.

The presence of oxygen in our samples has been detected by exciting the vibrational modes using FTIR technique. It has been reported that the presence of O_i is manifested by the absorption bands 1205, 1106 and 515 cm^{-1} [19]. The investigation of the 515 cm^{-1} band has led Shimura et al [20] suggest that (O_i) may be forming chainlike structures in Si lattice. Another reported value for O_i is at 1107 cm^{-1} at room temperature [21].

In our CZ-grown silicon sample (silicon 522 Big), we have also observed absorption peaks at 1107 cm^{-1} and 513.2 cm^{-1}. These peaks clearly indicate the presence of interstitial oxygen (Oi) in our Cz-grown sample. These features are shown in Fig. 4.2.

In our float-zone (FZ) samples, these peaks are totally disappeared. As discussed earlier in chapter 3 that float-zone technique is a zone refining technique. In this technique a part of the material is melted at a given instant, and a liquid zone is formed, which is moved along a long solid charged rod. As the liquid zone moves through the materials, the impurities are driven along with the liquid, and ultimately impurities reach at the end of the bar, which can than be cut off. Thus, this technique results in a considerable purification.

Therefore, it is well known that in the float-zone growth technique, the oxygen concentration is much smaller than in the CZ-grown samples. This fact is confirmed by comparing the FTIR absorption spectra taken by us both for CZ-grown and float-zone silicon crystals.

4.3.2 Effects of Carbon Concentration on Vibrational Modes.

The other common incorporated impurity, which arises during crystal growth in silicon, is carbon. Carbon atoms normally occupy substitutional lattice sites (Cs) [22]. It has been observed that three isotopes of carbon, namely an isolated carbon impurity C^{12}, C^{13}, and C^{14} give rise to three absorption bands at 604.9, 586.3 and 570.3 cm^{-1} respectively at room temperature [15]. Another reference [23], puts the value for C^{12} at 605 cm^{-1} at room temperature.

In our FTIR spectra, we have observed a strong Cs absorption peak at 605 cm^{-1} only in the Si HCLO sample, as shown in the Fig. 4.12. In this sample the concentration of carbon ($2 \times 10^{17} cm^{-3}$) is very high whereas oxygen concentration is

comparatively low. In all other samples, this peak is not very clear, only a hump is present in the vicinity of 605 cm-1 in almost all the spectra. These features can be seen in the figures of section 4.2.

4.3.3 Five Smaller Peaks

About five smaller peaks at around 576 cm^{-1}, 739 cm^{-1}, 818 cm^{-1}, 889 cm^{-1} and 962 cm^{-1} are present in all FTIR spectra, taken on both CZ-grown and float-zone silicon samples. There is a fair consistency in the appearance of these peaks. There is neither a considerable shift in the wavenumbers nor a change in the shape of these peaks.

It has been suggested [22] that a peak at 570 cm^{-1} is due to C^{14}. So the peak observed in our spectra at 567 cm^{-1} may be attributed to C^{14}. However, due to their low intensity of these smaller peaks no definite identification can be made for these peaks.

It is reported [24] that the second harmonic transitions due to B^{11} in silicon gives an absorption peak at 1238.5 cm^{-1} at room temperature. Therefore, the peak at 1233.6 cm^{-1} in Fig. 4.8 may be attributed to second harmonic transition due to B^{11} in sicilon.

4.3.4 The 610 cm^{-1} Peak

In our FTIR absorption spectra, the most prominent peak is at about 610 cm^{-1}. This feature is present in all our samples investigated. There is a shoulder at around 620 cm^{-1} and a hump at about 605 cm^{-1} on the low wavenumber side of this peak. We

have already mentioned that the hump at 605 cm^{-1} is probably due to the presence of Cs in the sample.

It has been suggested that naturally occurring boron consists of two isotopes present in abundnces of 18.8% and 81.2% for B^{10} and B^{11} respectively. These give rise to the absorption bands at 644.4 cm^{-1} and 620.6 cm^{-1} respectively at room temperature [15]. Thus we can say that the shoulder at 620 cm^{-1} is due to the presence of B^{11} in the silicon samples. It has been reported that the observed and calculated values of the local modes of vibration of a pair (B^{11}–B^{11}) of boron are 615 cm^{-1} and 612.5 cm^{-1} [25] respectively. Therefore, the peak at 610 cm^{-1} may be attributed to (B^{11}–B^{11}). It has also been suggested [26] that boron paired with antimony (B^{11}–Sb) gives an absorption peak at 612 cm^{-1}.So the peak at 610 cm^{-1} may be attributed to (B^{11}–Sb).

4.4 Conclusions

We have investigated the vibrational modes of oxygen, carbon and boron in silicon samples grown by Czochralski (CZ) and Float-zone (FZ) techniques using Fourier Transform Infrared (FTIR) absorption spectroscopy in the wavenumber range from 4600-400 cm^{-1}. All the measurements were performed at room temperature. After a thorough analysis and comparison with the available literature , we have arrived at the following conclusions:

1. The absorption peaks at 1107 cm^{-1} and 513.2 cm^{-1} in CZ silicon sample, represent the presence of interstitial oxygen (Oi) in silicon.

   These peaks are not present in Float-zone (FZ) silicon samples.

2. The peak at 605.7 cm^{-1}, in our Si HCLO sample, is attributed to the substitutional carbon (Cs) in the sample.
3. The 610 cm^{-1} peak present in almost all our spectra, may be attributed to pairs of boron (B^{11}-B^{11}) or may be due to the presence of boron paired with antimony (B^{11}-Sb). This peak has a shoulder to the left at about 620 cm^{-1} and a hump at around 605 cm^{-1} to the right. The shoulder at 620 cm^{-1} is due to B^{11} and a hump at 605 cm^{-1}, as mentioned earlier, is due to Cs.
4. Regarding the five smaller peaks, observed at 567.5, 739.8, 818, 890, and 962.5 cm^{-1}, the peak at 567.5 cm^{-1} may be attributed to C^{14}. The other peaks have not been identified definitely due to their lower intensities.
5. The absorption peak at about 1087.5 cm^{-1}, which only appears in Si Ref UHP oil quenched sample, may be attributed to the (C-O) pair.

Further work, obviously, is desirable at low temperatures to enhance and complement our analysis of the study of the vibrational modes in silicon using FTIR technique. This project can be undertaken, as a separate study, at a later stage in future.

REFERENCES

1 Dr. A. Rehman, Dr. M. Younis, Spectroscopy, University of Punjab, Lahore

2 Beiser, Perspectives of Modern Physics, McGraw-Hill Book Company.

3 Nicolet Manual, Introduction to Fourier Transform Infrared Spectrometry.

4 R. C. Newman, Infrared Studies of Crystal Defects, Taylor & Francis 10-14 Macklin Street, London (1973)

5 O' Mara W.C. in Defects in Silicon ed. M. W. Bullis and L. C. Kimerling (Princeton, NJ: Electrochemical Society) p 120.(1983)

6 C. A. Londs, Phys. Rev. B, **37**, 8, 4175 (1988).

7 John. R. Ferraro, Louis J. Basile. Fourier transform infrared spectroscopy, (application to chemical system), Vol. **1**, Academic Press,Inc., San Diego New York, London, Tokyo, Toronto.

8 Karl Dieter Moller, Walter G. Rothschild, Far-Infrared spectroscopy, Wiley-Interscience. (1971).

9 George A. Vanasse, Spectrometric Techniques. vol. 1, Academic Press, New York, San Francisco, London. (1977).

10 Rudolf Kings Lake, Applied optics and optical engineering, Academic Press New York & London, vol. 1 (1965).

11 Nicolet Manual, Introduction to Fourier transform infrared spectroscopy.

12 Donald A. Neaman, Semiconductor Physics and Devices, Richard D. Irwin, Inc., (1992).

13 C.H.L. Goodman, Crystal Growth Theory and Techniques, vol. 1.

14 Nicolet, Manual DX Reference/Operation (1986).

15 C.A. Londos. Semicond. Sci. Technol. **5**, 645, (1990).

16 O'Mara WC in Defects in Silicon ed. MW Bullis and L.C. Kimorling (Princeton, NI: Electrochemical Society), 120. (1983)

17 Gosele U and Tan T Y 1982 Appl. Phys. A (28), 79.

18 Murin L I and Markevich VP 1988 Sov. Phys. Semicond. (22), 840.

19 Wilkes JW 1988 in Properties of Silicon (EMIS Data Yeview Series No.4). London, IEE)(.281.

20 F. Shimura, Y. Ohnishi, and H. Tsuya, Appl. Phys. Lett. **38**, 867 (1981).

21 A. Baghdadi et al., J. Electrochem. Soc. **136**, 2015, (1989).

22 Newman, R.C., and Smith, R.S., J. Phys. Chem. Solids, **30**, 1493 (1969).

23 R.C. Newman and J.B. Willis, J. Phys. Chem. Solide, **26**, 373 (1965).

24 Angress et al., Proc. R. Soc. A. **287**, 64 (1965).

25 Newman, R.C., and Smith, R.S., Physics Lett. A, **24**, 671 (1967a);

26 Newman, R.C., Smith, R.S., Localized Excitations in Solids, edited by R.F. Wallis (New York; Plenum Press), 177 (1968).